



# GDNF enhances human blood-nerve barrier function *in vitro* via MAPK signaling pathways

Chaoling Dong and Eroboghene E. Ubogu

Neuromuscular Immunopathology Research Laboratory, Division of Neuromuscular Disease, Department of Neurology, University of Alabama at Birmingham, Birmingham, AL, USA

## ABSTRACT

The human blood-nerve barrier (BNB) formed by endoneurial microvascular endothelial cells, serves to maintain the internal microenvironment in peripheral nerves required for normal axonal signal transduction to and from the central nervous system. The mechanisms of human BNB formation in health and disease are not fully elucidated. Prior work established a sufficient role for glial-derived neurotrophic factor (GDNF) in enhancing human BNB biophysical properties following serum withdrawal *in vitro* via RET-tyrosine kinase-dependent cytoskeletal remodeling. The objective of the study was to ascertain the downstream signaling pathway involved in this process and more comprehensively determine the molecular changes that may occur at human BNB intercellular junctions under the influence of GDNF. Proteomic studies suggested expression of several mitogen-activated protein kinases (MAPKs) in confluent GDNF-treated endoneurial endothelial cells following serum withdrawal. Using electric cell-substrate impedance sensing to continuously measure transendothelial electrical resistance and static transwell solute permeability assays with fluoresceinated small and large molecules to evaluate BNB biophysical function, we determined MAPK signaling was essential for GDNF-mediated BNB TEER increase following serum withdrawal downstream of RET-tyrosine kinase signaling that persisted for up to 48 hours *in vitro*. This increase was associated with reduced solute permeability to fluoresceinated sodium and high molecular weight dextran. Specific GDNF-mediated alterations were detected in cytoskeletal and intercellular junctional complex molecular transcripts and proteins relative to basal conditions without exogenous GDNF. This work provides novel insights into the molecular determinants and mechanisms responsible for specialized restrictive human BNB formation in health and disease.

## ARTICLE HISTORY

Received 4 June 2018  
Revised 29 October 2018  
Accepted 7 November 2018

## KEYWORDS

Blood-nerve barrier (BNB); electric cell-substrate impedance sensing (ECIS); endoneurial endothelial cells; glial-derived neurotrophic factor (GDNF); human peripheral nerves; PCR arrays; proteomics; solute permeability; transendothelial electrical resistance (TEER)


## Introduction

Tight regulation of water, ion, nutrient, metabolite and xenobiotic concentrations within peripheral nerves is critical to maintaining the internal microenvironment needed for physiologic axonal signal transmission.<sup>1-3</sup> The blood supply to human nerves is derived from extrinsic arteries known as the vasa nervosum. These vessels subsequently branch to form a macrovascular anastomosis within the external epineurium and smaller diameter vessels within the concentric multilayered perineurium. The latter vessels penetrate the innermost perineurium to form endoneurial microvessels. In contrast to the highly permeable fenestrated epineurial blood vessels that lack tight junctions, the endoneurial microvasculature lack

fenestrations and consist of tight junction-forming endothelial cells. These cells share a basement membrane with pericytes which form a non-continuous surrounding layer along the endothelial cell abluminal border.<sup>4,5</sup> As a consequence, endoneurial microvessels form the BNB, as these endothelial cells are in direct contact with circulating blood. Current knowledge of the molecular and biophysical characteristics of the human BNB *in vitro*, including measures of transendothelial electrical resistance (TEER), solute permeability to small and large molecules, and response to cytokine and mitogen stimulus has been recently summarized.<sup>6</sup> Comprehensive data on the molecular composition of the human BNB based on RNA sequencing has also been recently published.<sup>7</sup>

**CONTACT** Eroboghene E. Ubogu  [eeubogu@uabmc.edu](mailto:eeubogu@uabmc.edu); [ubogu@uab.edu](mailto:ubogu@uab.edu)  Division of Neuromuscular Disease, Department of Neurology, University of Alabama at Birmingham, 1720 7th Avenue South, Sparks Center Suite 200, Birmingham, AL 35294-0017, USA

Color versions of one or more of the figures in the article can be found online at [www.tandfonline.com/ktib](http://www.tandfonline.com/ktib).

 Supplemental data for this article can be accessed [here](#).

© 2018 Taylor & Francis

GDNF, a related member of the transforming growth factor  $\beta$  protein superfamily, supports the survival of peripheral autonomic and sensory, spinal cord motor and midbrain dopaminergic neurons.<sup>8-12</sup> GDNF typically signals via its glycosylphosphatidylinositol-anchored protein receptor, GFR $\alpha$ 1, complexed with “rearranged during transfection” (RET)-tyrosine kinase as part of a multicomponent receptor complex, and utilizes intracellular Ras-mitogen activated protein kinase (MAPK), phosphatidylinositol 3-kinase (PI3-K)/AKT, p38 MAPK and c-Jun N-terminal kinase signaling pathways for its biological effects.<sup>11,13-17</sup> Primary human endoneurial endothelial cells (pHEndECs) that form the BNB express GFR $\alpha$ 1 *in vitro* and *in situ*.<sup>7,18-20</sup> Our prior work demonstrated that GDNF is a sufficient paracrine human BNB regulator following serum withdrawal *in vitro*.<sup>19</sup>

GDNF (in a dose-dependent manner) induced restrictive human BNB properties dependent on RET-tyrosine kinase signaling pathways via histologically-observed cytoskeletal reorganization (i.e. translocation of F-actin cytoskeletal filaments from the cytoplasm to cell membranes) that resulted in more continuous intercellular contacts. This occurred without significantly upregulating known adaptor, adherens and tight junction-associated protein expression, or modulating claudin-5 phosphorylation *in vitro*, and was independent of cyclic AMP/protein kinase A signaling.<sup>19</sup> That study also suggested a role for hyperactivated MAPK signaling in GDNF-mediated human BNB recovery when combined with other less efficacious mitogens (in an attempt to mimic *in vivo* conditions), with published preliminary data further supporting a direct role of MAPK signaling in GDNF-mediated restoration of human BNB electrical resistance.<sup>21</sup>

A role for GDNF in regulating microvascular endothelial and epithelial tight junction barrier function had also been described in mammalian blood-brain, blood-retina, blood-testis and intestinal barriers *in vitro* or *in vivo*,<sup>20,22-28</sup> in addition to the human *in vitro* BNB. In order to ascertain the signaling pathways by which GDNF enhances human BNB function *in vitro* following serum withdrawal downstream of RET-tyrosine kinase, we performed electric cell-substrate impedance sensing (ECIS) to continuously monitor impedance, TEER and capacitance,<sup>29</sup> and transwell solute permeability assays to fluoresceinated

low and high molecular weight molecules using specific cell permeable signaling pathway inhibitors, guided by proteomic data derived from GDNF-treated pHEndECs following serum withdrawal *in vitro*, with appropriate controls. To more comprehensively ascertain potential molecular determinants of the intercellular junctional complex responsible for the previously ascertained GDNF-mediated effect on the restrictive human *in vitro* BNB, we performed human adherens junction and tight junction quantitative real-time polymerase chain reaction (PCR) arrays, quantitative proteomics of cytosolic and membrane protein extracts and fluorescent indirect immunocytochemistry on confluent pHEndEC cultures 48 hours following serum withdrawal with and without added GDNF.

## Results

### **Serum withdrawal induces pHEndEC cytoskeletal changes and more organized and continuous intercellular contacts at the human BNB *in vitro***

Prior to serum withdrawal, visually appearing confluent pHEndECs cultured in regular growth medium consisted of both actively dividing cuboidal-shaped cells with larger cytoplasm-to-nucleus ratios and non-dividing, more compact spindle-shaped cells (Figure 1A). Several hours following serum withdrawal, majority of the cells appeared spindle-shaped with more compact cytoplasm and more defined contrast (phase bright) between cells. 48 hours following serum withdrawal in basal medium lacking GDNF, pHEndEC layers appeared less organized (Figure 1B) relative to pHEndEC layers treated with GDNF (Figure 1C). These observations were supported by larger cytoplasm with more diffuse intracytoplasmic F-actin cytoskeletal filaments and more frequent intercellular gaps prior to serum withdrawal (Figure 1D) compared to more compact cytoplasm with F-actin cytoskeletal filaments more localized at the interendothelial cell membranes (Figures 1E and F). In addition, GDNF-treated pHEndEC layers appeared more organized with more uniformly appearing cells and fewer intercellular gaps 48 hours following serum withdrawal (Figure 1F) compared to untreated cells (Figure 1E).

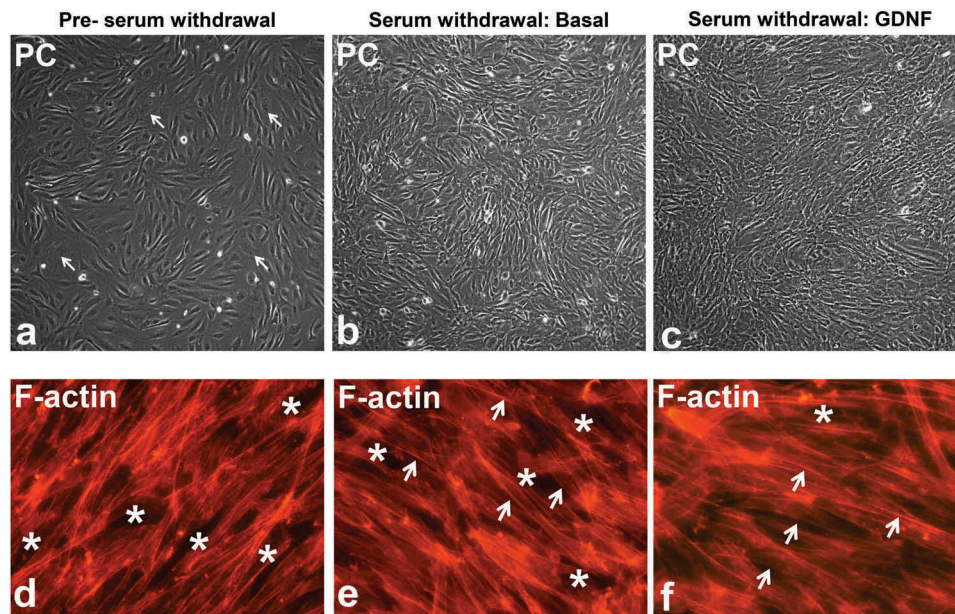


**Figure 1.** GDNF-mediated human BNB morphological changes following serum withdrawal. Representative phase contrast digital photomicrographs of visually confluent pHEndECs *in vitro* following initial seeding and culture in regular growth medium (A) and following serum withdrawal in basal medium (B) and basal medium containing 1 ng/mL GDNF (C) demonstrate an admixture of proliferating cuboidal-shaped (white arrows) and spindle-shaped cells prior to serum withdrawal. Diffuse spindle-shaped endothelial cells are characteristic following serum withdrawal, with endothelial layers appearing more organized 48 hours afterwards in the presence of GDNF (C) compared to basal conditions (B). Intercellular gaps (white asterisk) and more cuboidal cells with larger cytoplasm and more diffuse intracytoplasmic F-actin cytoskeletal filaments are more commonly seen prior to serum withdrawal (D). Spindle-shaped cells with more F-actin localization at intercellular membranes (white arrows) are more prevalent following serum withdrawal (E, F) with fewer intercellular gaps (white asterisk) seen following GDNF treatment 48 hours afterwards. PC = Phase Contrast. Initial magnification 100X (A-C) and 400X (D-F).

### **Intracellular MAPK proteins, MEK1/2 and ERK1/2 are detected in GDNF-treated confluent pHEndECs following serum withdrawal**

Liquid chromatography-mass spectrometry (LC-MS) analysis of pHEndEC cytoplasmic protein extracts following trypsin digestion of the 10% Bis-Tris gel stained with Colloidal Coomassie overnight (Figure 2) identified 1068 proteins, including dual specific MAPK2K2 (MEK1/2) and MAPK3 (ERK1/2), as shown in Supplementary File 1. These data imply that downstream MAPK signaling may be relevant to the observed and previously published GDNF-mediated pHEndEC cytoskeletal modifications and human BNB TEER enhancement following serum withdrawal *in vitro* that was dependent on RET-tyrosine kinase signaling.<sup>19</sup> Cytoskeletal and junctional complex proteins implicated in specialized intercellular junction formation were also identified. These include ACTN1, ACTN4, PARVA, CTNNA1, DSP, FLNA, FLNB, FLNC, LASP1, PDLIM1, SPTAN1, TJP1 (ZO-1), TJP2 (ZO-2), TLN1 and ZYX.

### **Inhibition of MAPK kinase signaling abrogates human BNB TEER increase following serum withdrawal**

Using ECIS to continuously measure TEER, GDNF (0.1–100 ng/mL) resulted in a dose-dependent increase in human BNB TEER following serum withdrawal *in vitro* relative to basal conditions, with maximal effect seen at 1 ng/mL (0.033 nM; data not shown), as previously established.<sup>19,21</sup> There was an initial exogenous GDNF-independent increase in TEER following serum withdrawal that lasted ~16–20 hours followed by a progressive decline in resistance under basal conditions (Figure 3). The exogenous GDNF-dependent phase started ~8 hours after serum withdrawal and resulted in maximal TEER at ~26–27 hours. The GDNF-induced increase in TEER persisted longer and with less decline observed 48 hours after serum withdrawal compared to basal conditions. Inhibitors against MEK1 and ERK1/2 completely inhibited the GDNF-mediated TEER increase down to basal levels by



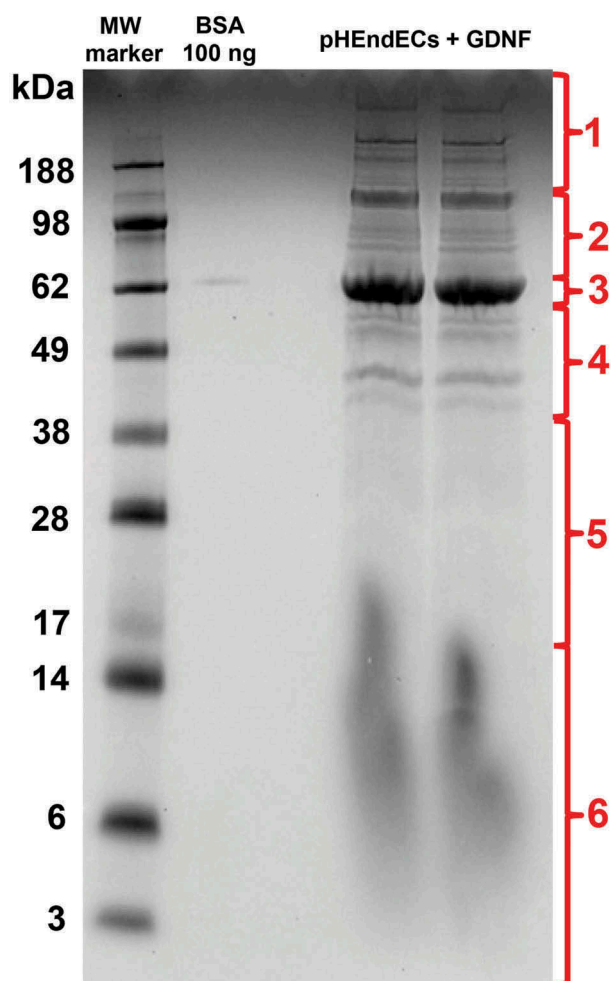


**Figure 2.** GDNF-treated pHEndEC protein expression following serum withdrawal. A digital photograph of the Colloidal Coomassie-stained 10% Bis-Tris gel following SDS-PAGE of pHEndEC protein extracts shows the six sections of the gel cut from top to bottom prior to trypsin digestion (indicated in red), with subsequent LC-MS, protein identification and GO annotation, as described in the Materials and Methods section. Unexpected vertical smearing is seen in both lanes containing pHEndEC cytoplasmic protein extracts < 20 kDa molecular weight.

48 hours following serum withdrawal while the RET-Tyrosine kinase inhibitor reduced the maximal TEER to basal levels with a lower decline compared to basal, MEK 1-inhibited and ERK1/2-inhibited conditions (Figure 3).

MEK1 and ERK1/2 blockade near completely abrogated the GDNF-mediated TEER increase down to basal levels based on the calculated mean absolute increase in TEER above baseline levels prior to serum withdrawal (Figure 4A) and % maximal TEER (persistence) relative to the maximal GDNF-enhanced TEER observed during serum withdrawal at 48 hours (Figure

4B). RET-tyrosine kinase inhibition resulted in a statistically significant higher mean TEER increase and persistence compared to basal, MEK1 and ERK1/2-inhibited conditions, suggesting that GDNF may partially signal via non-RET-tyrosine kinase signaling pathways and utilize downstream MAPK-dependent intracellular signaling pathways to maintain elevated TEER following serum withdrawal *in vitro*. There were no significant differences in capacitance (a measure of endothelial cell coverage over the recording electrodes)<sup>29</sup> between the treatment groups (Figure 5), implying that GDNF did not induce a change in pHEndEC density following serum withdrawal, consistent with our prior published observations that demonstrated a weak GDNF effect on pHEndEC proliferation (based on a sensitive non-radioactive tetrazolium salt, WST-1 proliferation assay) and angiogenesis (based on a 4 hour Matrigel<sup>TM</sup> assay) *in vitro*.<sup>18</sup>

Overall, these data support the hypothesis that GDNF enhances human BNB TEER following initial confluent pHEndEC culture and serum withdrawal, dependent on RET-tyrosine kinase/MAPK signaling pathways *in vitro* without significant change in endothelial cell proliferation, using capacitance as a surrogate marker. The initial GDNF-independent increase in TEER was temporally associated with pHEndEC cytoskeletal changes that resulted in more compact spindle-shaped pHEndECs (which may increase transcellular TEER) and more continuous intercellular contacts (which should increase junctional or paracellular TEER). The partial increase in TEER seen under basal conditions without exogenous GDNF suggests transient autocrine activity of GDNF or other redundant mitogens (e.g. transforming growth factor- $\beta$ 1, basic fibroblast growth factor) that are biologically insufficient to maintain a high TEER. Subsequent development of cytoskeletal retraction and less continuous intercellular contacts as demonstrated by phase contrast microscopy and F-actin immunohistochemistry may occur as early as ~ 16–20 hours following serum withdrawal and progressively worsen over 48 hours, consistent with previous work evaluating RET-tyrosine kinase signaling following GDNF treatment.<sup>19</sup>

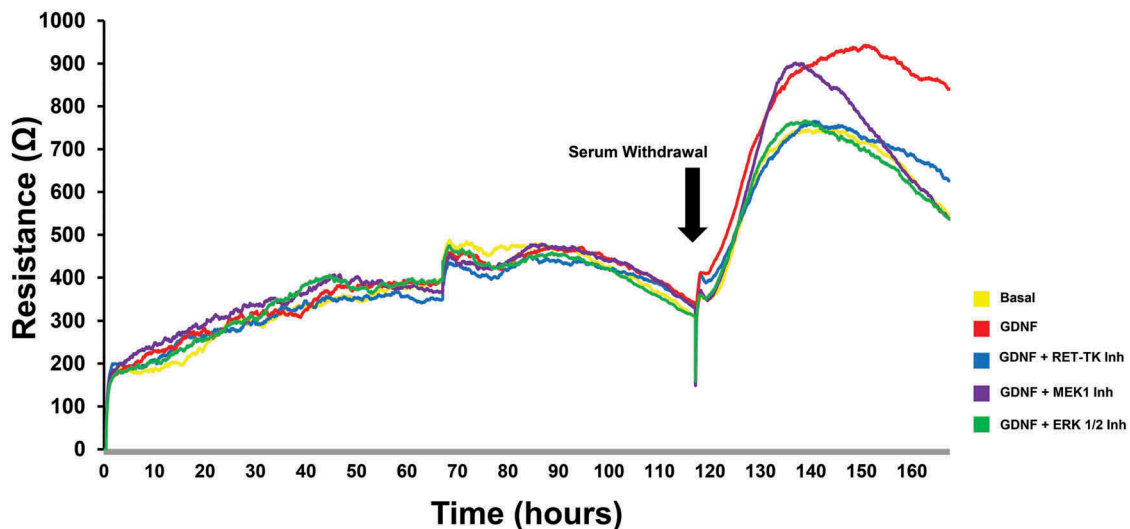


**Figure 3.** GDNF effect on transendothelial electrical resistance. A representative graph of continuous human BNB TEER measured by ECIS obtained from a single experiment shows the uniform gradual increase in TEER in regular growth medium. Serum withdrawal is associated with an initial increase in resistance that peaks in ~ 16–20 hours with progressive decline until the end of the experiment 48 hours afterwards under basal conditions. GDNF results in a higher TEER that peaks ~ 26–27 hours after serum withdrawal with less decline 48 hours afterwards. Specific inhibitors against RET-tyrosine kinase (RET-TK Inh), MEK1 (MEK1 Inh) and ERK1/2 (ERK 1/2 Inh) abrogate the GDNF-mediated TEER changes.

### ***Inhibition of MAPK kinase signaling modulates reduction in human BNB solute permeability following serum withdrawal***

GDNF significantly reduced solute permeability to Na-FITC (Figure 6A) and dextran-70-FITC (Figure 6B) 48 hours after serum withdrawal when normalized and compared to the untreated (basal) condition. This effect was abolished by specific cell-permeable inhibitors against RET-tyrosine kinase, MEK1 and ERK1/2, with no significant differences observed between these inhibitors and basal conditions. The mean solute permeability to Na-FITC following serum withdrawal under basal conditions was  $10.89 (\pm 4.54)\%$ , with a reduction to  $6.91 (\pm 2.00)\%$  following 1 ng/mL GDNF treatment. The mean Na-FITC permeabilities following serum withdrawal with concurrent treatment with GDNF and specific inhibitors of RET-tyrosine kinase, MEK1 and ERK1/2 were  $11.25 (\pm 3.22)\%$ ,  $9.57 (\pm 2.97)\%$  and  $11.70 (\pm 3.60)\%$  respectively and were not different from basal conditions. The mean solute permeability to dextran-70-FITC following serum withdrawal under basal conditions was  $2.61 (\pm 1.39)\%$ , with a reduction to  $1.93 (\pm 0.94)\%$  following GDNF treatment. The mean dextran-70-FITC permeabilities following serum withdrawal and concurrent treatment with GDNF and specific inhibitors

of RET-tyrosine kinase, MEK1 and ERK1/2 were  $2.95 (\pm 1.18)\%$ ,  $2.54 (\pm 1.20)\%$  and  $2.54 (\pm 1.06)\%$  respectively, and were not different from basal conditions based on normalized values under basal conditions without exogenous GDNF treatment.

These data support the hypothesis that GDNF enhances the restrictive human BNB biophysical property of limiting paracellular transport of small and large molecules via RET-tyrosine kinase/MAPK signaling mechanisms following serum withdrawal. This is consistent with previously published initial observations of GDNF-mediated reduction in dextran-70-FITC permeability following serum withdrawal, as well as the observed more continuous intercellular contacts and fewer intercellular gaps (that may provide a route for paracellular transport or diffusion) between adjacent pHEndECs mediated by GDNF and RET tyrosine kinase following serum withdrawal *in vitro*.<sup>19</sup>

### ***GDNF facilitates persistent increase in human BNB biophysical properties via specific changes in the cytoskeletal-intercellular adherens and tight junctional complex***

Upregulation in specific adherens and tight junctional complex gene expression following GDNF

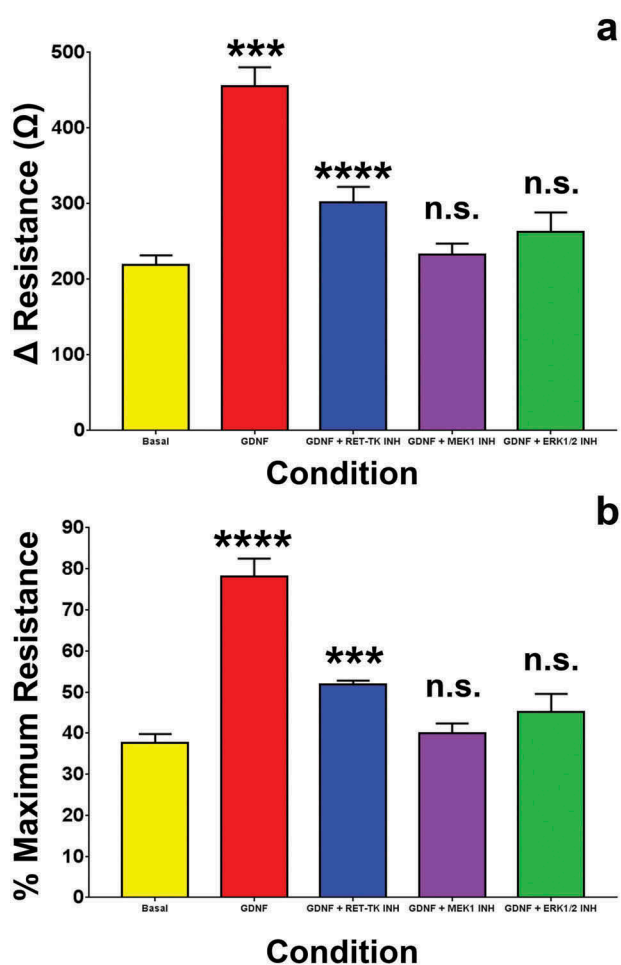


**Figure 4.** GDNF effect on BNB TEER recovery following serum withdrawal. Bar histograms demonstrate that GDNF significantly enhanced human BNB restrictive biophysical properties based on maximal calculated absolute TEER increase (A) and % maximal TEER (persistence) at 48 hours following serum withdrawal (B). Inhibitors against MEK1 (MEK1 INH) and ERK1/2 (ERK 1/2 INH) completely abrogated the GDNF-mediated resistance enhancement with no significant differences compared to basal conditions without added GDNF, while an inhibitor against RET-tyrosine kinase (RET-TK INH) resulted in a small, but statistically significant partial effect relative to basal conditions. \*\*\* indicates  $p < 0.001$ , \*\*\*\* indicates  $p < 0.0001$  and n.s. indicates not significant.  $N = 3$  independent experiments in triplicate.

treatment may indicate the changes required to develop or restore the restrictive biophysical properties at the human BNB, while reduced expression relative to basal conditions may indicate transcripts downregulated after forming the restrictive junctional complex or compensatory transcripts highly expressed by the BNB in an attempt to develop and maintain restrictive barrier function in the absence of exogenous GDNF.

The Human Adherens Junction PCR array demonstrated that the GDNF-mediated increase in

the human BNB restrictive biophysical properties following serum withdrawal was significantly associated with increased expression of the following top 5 gene transcripts: *CDH3* (adherens junction protein; 44607.5-fold), *ACTN2* (cytoskeletal protein; 2452.4-fold), *CTNNA3* (adaptor protein linking cytoskeleton to adherens junction; 448.8-fold), *CDH1* (adherens junction protein; 221.3-fold) and *CTNNA2* (adaptor protein; 23.6-fold). Decreased expression of the following top 5 gene transcripts was also observed: *DSG3*, *DSC3* (desmosome proteins; 495.4-fold and 284.1-fold respectively), *PVRL4* (adherens junction protein; 254.7-fold), *SSX2IP* and *SORBS1* (adaptor proteins; 181.7-fold and 169.2-fold respectively), as shown in Figure 7.

GDNF-mediated increased transcript expression of cytoskeletal component or regulatory genes *ACTN2*, *RALA*, *WASL*, *ARF6*, *TLN1*, *ACTN3*, and *WAS* with reduced expression of *WASF1*, *RAC1*, *MAPRE1*, *ZYX* and *IQGAP1* relative to basal conditions following serum withdrawal was detected. Increased expression of adaptor components *CTNNA3*, *CTNNA2* and *CTNNA1* with reduced expression of *SSX2IP*, *SORBS1*, *JUP* (*CTNNG*) and *PKP2* was also observed. Changes in several regulators of cellular function such as plasma membrane remodeling (increased: *HGS*; decreased: *CSNK2B*, *PIK3CG*), apoptosis (increased *PERP*, *CSNK2A2*), and cell polarity and intercellular communication (decreased *DLL1*, *PARD3*) were also observed following GDNF-mediated enhancement of human BNB restrictive biophysical properties following serum withdrawal *in vitro*.

In terms of adherens junction and desmosome components, there was GDNF-mediated increased expression in *CDH3*, *CDH1*, *DSG1*, *DSC2*, *PVRL2*, *PVRL3* and *PVRL1*, with reduced expression of *DSG3*, *DSC3*, *PVRL4*, *DSG4*, *CDH4*, *DSG2*, *DSC1*, *VEZT* and purinergic receptor *P2RX6* (which interacts with *CDH5* at adherens junctions *in vitro*)<sup>30</sup> relative to basal conditions. The relative high expression of specific desmosome transcripts under basal conditions following serum withdrawal (Figure 7) suggests possible intercellular desmosome formation as compensation by the *in vitro* human BNB in an attempt to develop a restrictive barrier in the absence of the observed GDNF-mediated increase in specific cytoskeletal-adaptor-adherens junction components potentially

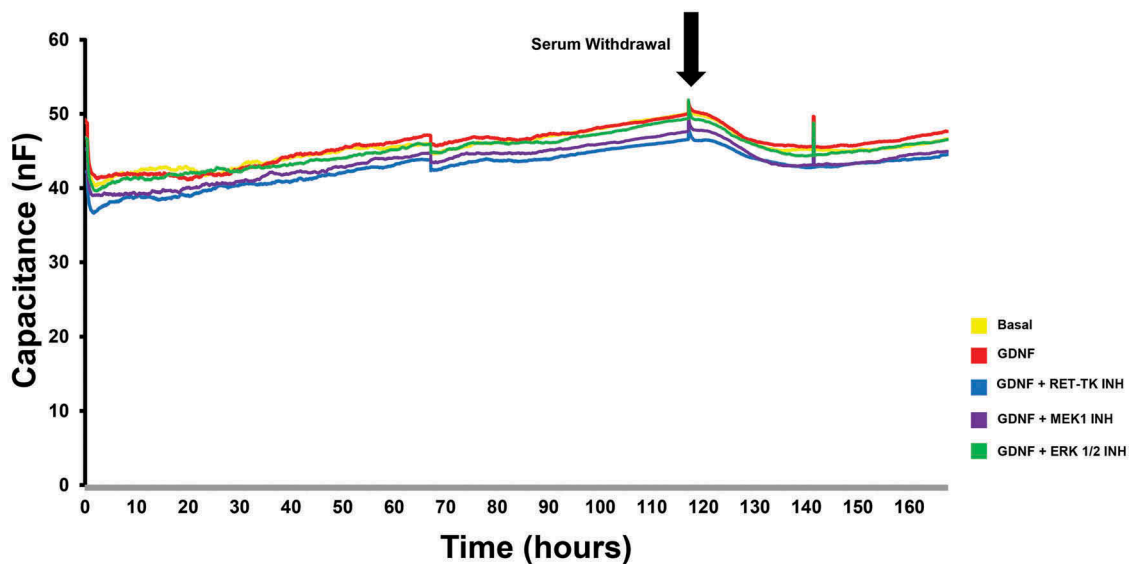


**Figure 5.** GDNF effect on transendothelial capacitance. A representative graph of continuous human BNB capacitance measured by ECIS obtained from a single experiment shows a slight uniform gradual increase in capacitance following sub-confluent pHEndEC culture in regular growth medium. Serum withdrawal is associated with an initial slight decrease in capacitance for ~8–12 hours that plateaus with no significant increase over the next 36–40 hours. No significant differences in capacitance are observed between basal and GDNF-treated confluent pHEndECs, and GDNF-treated pHEndECs with specific inhibitors against RET-tyrosine kinase (RET-TK Inh), MEK1 (MEK1 Inh) and ERK1/2 (ERK 1/2 Inh) following serum withdrawal.

associated with the highly restrictive intercellular junctional complex and BNB biophysical properties. However, it is important to recognize that endothelial cells lack typical desmosomes and that transcripts expressed may not undergo translation to functional protein or expression at intercellular junctional membranes.

The Human Tight Junction PCR array demonstrated that the GDNF-mediated increase in human BNB restrictive biophysical properties was significantly associated with increased expression of the following top 5 gene transcripts: *CTNNA2* (adaptor protein; 2645300.2-fold), *ACTN3* (cytoskeletal protein; 106883.2-fold), *CRB3* (tight junction formation regulator; 1013.4-fold), *CLDN19* (tight junction protein; 476.1-fold) and *CGN* (tight junction adaptor protein; 360.8-fold). Decreased expression of the following top 5 gene transcripts was also observed: *PARD6B* (cell polarity regulator; 907.0-fold), *PRKCZ* (serine/threonine kinase cell function regulator; 404.5-fold), *CLDN8*, *CLDN4* (tight junction proteins; 188.7-fold and 155.4-fold respectively), and *SPTA1* (cytoskeletal component; 88.0-fold), as shown in Figure 8.

GDNF-mediated increased transcript expression of cytoskeletal component or regulatory genes *ACTN3*, *LLGL1*, *HCLS1*, *SPTAN1*, *SPTB*, *LLGL2*, *ACTN1*, *EPB41* and *ACTN4* with reduced expression of *SPTA1* relative to basal conditions following serum withdrawal was detected using this array. Increased expression of adaptor components *CTNNA2*, *CGN*, *CTNNA3*, *CTNNB1* and *CTNNA1* was also observed. Changes in several regulators of cellular function such as regulation of cell polarity (increased *PARD6A*, *MARK2*, *SMURF1*, *MPP5*, *MPDZ* and *PARD3*; decreased *PARD6B*), specific serine/threonine kinases (increased *CDK4*, decreased *PRKCZ*), cell adhesion molecules/attachment regulators (increased *ICAM2*, *ILK*, *ICAM1*) were also observed following GDNF-mediated enhancement of human BNB restrictive biophysical properties following serum withdrawal *in vitro*. In support of our prior hypothesis that exogenous GDNF mediates the development of restrictive BNB tight junction properties via cytoskeletal remodeling and formation of more continuous intercellular junctions, increased expression of *ARHGEF2* (involved in exogenous Rho-GTPase signaling pathways) and *ESAM* (involved in



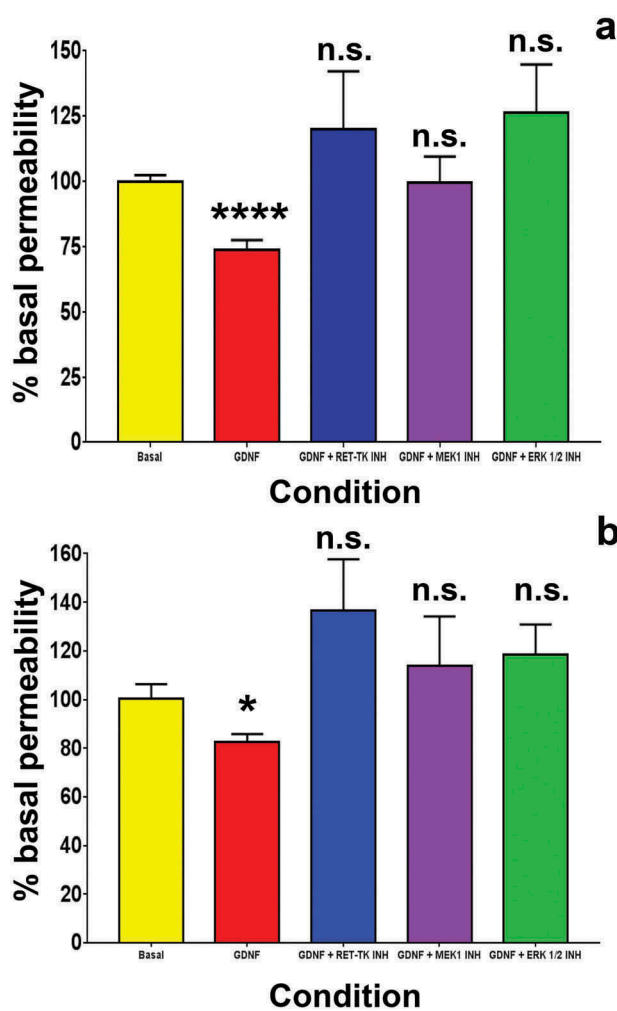


**Figure 6.** GDNF effect on BNB solute permeability following serum withdrawal. Bar histograms demonstrate that GDNF significantly reduced human BNB solute permeability to Na-FITC (A) and dextran-70-FITC following serum withdrawal (B). Inhibitors against RET-tyrosine kinase (RET-TK INH), MEK1 (MEK1 INH) and ERK1/2 (ERK 1/2 INH) completely abrogated the GDNF-mediated permeability reduction with no significant differences compared to basal conditions without added GDNF. \* indicates  $p < 0.05$ , \*\*\*\* indicates  $p < 0.0001$  and n.s. indicates not significant.  $N = 5$  independent experiments in triplicate.

formation of continuous intercellular junctions by correcting intercellular membrane gaps)<sup>31</sup> were also observed.

In terms of tight junction protein and junctional regulatory components, there was GDNF-mediated increased expression in *CRB3*, *CLDN19*, *CLDN2*, *CLDN3*, *CRB1*, *F11R*, *AMOTL1*, *TJAP1*, *CLDN14*, *TJP1*, *JAM3*, *ASH1L*, *MAGI1*, *MLLT4*, *TJP2*, *CLDN1*, *SYMPK*, *CD99*, *CTTN* and *CLDN16*, with reduced expression of *CLDN8*, *CLDN4*, *CLDN5* and *IGSF5* (*JAM4*) relative to basal conditions. The relative high expression of

a few specific claudin transcripts and a cytoskeletal component under basal conditions following serum withdrawal (Figure 8) may imply a compensatory attempt to form or maintain restrictive tight junctions by these endothelial cells in the absence of exogenous GDNF or down-regulation of these specific transcripts following GDNF-mediated development of a more restrictive tight intercellular junctional complex via increased expression of specific cytoskeletal-adaptor-cell-polarity regulator-tight junction components following serum withdrawal after initial endothelial monolayer formation *in vitro*. It is important to emphasize that specific transcripts expressed by the human *in vitro* BNB induced by exogenous GDNF treatment may not be translated to functional proteins involved in cytoskeletal-intercellular junctional complex formation or expressed in the appropriate subcellular location required to establish restrictive tight junctions, and differences may exist compared to the *in vivo* human BNB.

### ***GDNF induces alterations in cytosolic and membrane expression of specific cytoskeletal and junctional complex-associated proteins***

LC-MS analysis of pHEndEC cytosolic and membrane protein extracts following trypsin digestion of the 10% Bis-Tris gel stained with Colloidal Coomassie overnight (Figure 9) identified 1054 proteins, including specific cytoskeletal-junctional complex associated proteins *ACTN1*, *ACTN4*, *CDC42*, *CDH2*, *CDH11*, *CDH13*, *CELSR1*, *CTNNA1*, *CTNNB1*, *CTNND1*, *DLG1*, *FLNA*, *FLNB*, *FLNC*, *LMO7*, *ICAM1*, *PARVA*, *PDZLIM1*, *PDZLIM 5*, *PDZLIM7*, *RAC1*, *SPTAN1*, *TJP1*, *TLN1*, *VAPA*, *VAPB*, *VCL*, *ZYX*, as shown in Supplementary File 2. Several “classic” adherens and tight junction associated proteins such as *CDH5*, *CLDN5*, *F11R* (also known as *JAM1*) and *OCN* were not detected using the predefined peptide/protein identification parameters. Surprisingly, *CTNNA2* was not detected in either the cytosolic or membrane fractions of GDNF-treated pHEndECs following serum withdrawal despite data implying significant upregulation in transcript expression from the Human Adherens and Tight Junction PCR arrays.



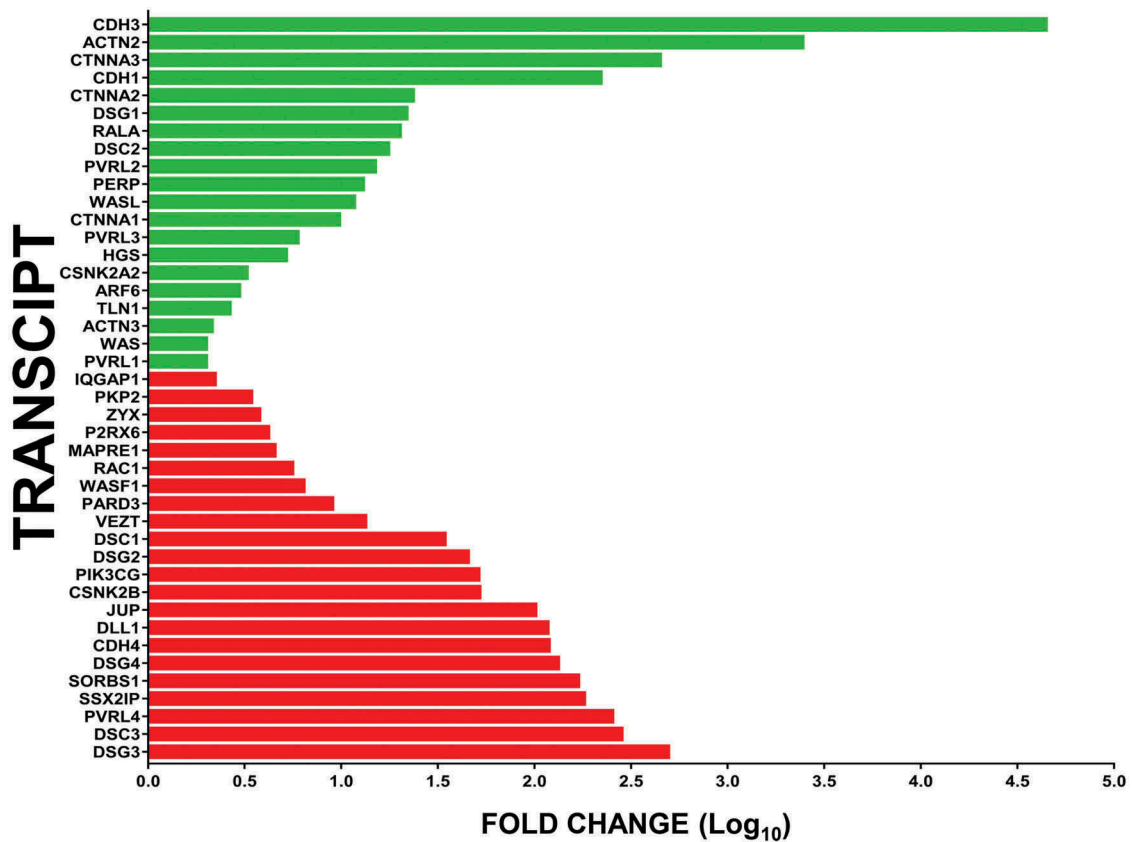


**Figure 7.** Effect of GDNF on human BNB adherens junctional complex transcripts following serum withdrawal. Bar histograms depict the mean fold-change in specific GDNF-mediated BNB adherens junction complex associated transcripts following serum withdrawal relative to basal conditions without exogenous GDNF, demonstrating the repertoire of cytoskeletal-adaptor-adherens junction component transcript changes associated with restrictive human BNB function *in vitro*. Green bars represent increased expression (in descending order of magnitude) while red bars represent decreased expression (in ascending order of magnitude) for statistically significant transcripts with fold-change  $\geq 2.0$ . Error bars are not included to improve clarity. N = 2 independent experiments in duplicate.

Comparative quantitative proteomics of GDNF-treated pHEndECs relative to basal (untreated) cultures demonstrated an increase in total CTNNA1 protein expression following GDNF treatment that was associated with an increased membrane fraction and reduction in the cytosolic fraction (Table 1). This implies GDNF-mediated CTNNA1 upregulation and translocation from the cytosol to intercellular membranes that was associated with more restrictive intercellular junctions. There was a global increase in TLN1 protein expression in both cytosolic and membrane fractions, while there was no significant difference in ZYX cytosolic protein levels between GDNF-treated and basal pHEndEC cultures with a reduction in membrane and total protein levels. This suggests a potential role for TLN1 in GDNF-mediated restrictive junctional complex formation

and a compensatory increase in membrane ZYX expression in basal cultures following serum withdrawal as a means to develop restrictive intercellular junctions in the absence of exogenous GDNF-mediated signaling (Table 1).

Immunocytochemistry of GDNF-treated pHEndECs further supported the absence of cytosolic or membrane CTNNA2, with expression restricted to nuclei in basal and GDNF-treated cells (Figure 10A and B). Foci of high cytoplasmic CTNNA1 expression was observed in basal cultures (Figure 10C) with more diffuse and higher membrane-associated expression seen in GDNF-treated pHEndECs (Figure 10D). Diffuse TLN1 expression seen in basal cultures (Figure 10E) was more intense following GDNF-treatment (Figure 10F), while foci of high ZYX expression associated with pHEndEC intercellular cytoplasmic projections was

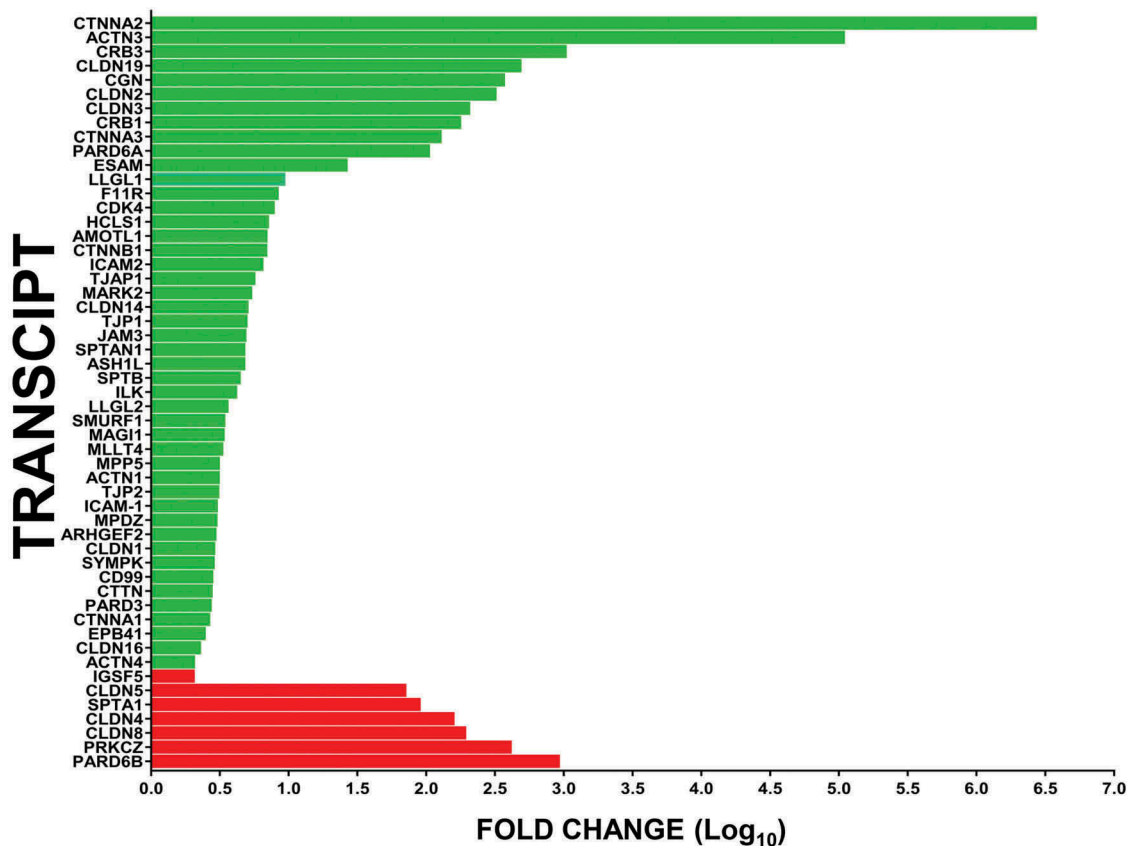


**Figure 8.** Effect of GDNF on human BNB tight junctional complex transcripts following serum withdrawal. Bar histograms depict the mean fold-change in specific GDNF-mediated BNB tight junction complex associated transcripts following serum withdrawal relative to basal conditions without exogenous GDNF, demonstrating the repertoire of cytoskeletal-adaptor-cell polarity-tight junction component transcript changes associated with restrictive human BNB function *in vitro*. Green bars represent increased expression (in descending order of magnitude) while red bars represent decreased expression (in ascending order of magnitude) for statistically significant transcripts with fold-change  $\geq 2.0$ . Error bars are not included to improve clarity. N = 2 independent experiments in duplicate.

observed under basal culture conditions (Figure 10G), with more diffuse and less intense expression observed following GDNF treatment (Figure 10H). These expression profiles were consistent with the PCR array and quantitative proteomic data.

Reduced *VEZT* transcript expression was observed in confluent GDNF-treated pHEndECs following serum withdrawal (Figure 7). *VEZT* was not detected by LC-MS analyses of the cytosolic or membrane fractions of either basal or GDNF-treated pHEndECs (see Supplementary File 2). However, immunocytochemistry using a specific primary antibody demonstrated increased focal perinuclear and cytosolic expression in GDNF-treated cells (Figure 10J) compared to basal cultures (Figure 10I), implying *VEZT* downregulation following GDNF-mediated restrictive intercellular junctional complex formation following protein transcription. Intercellular

membrane detection of TJP1, CDH5 and CLDN5 were also observed on basal and GDNF-treated pHEndECs (Figures 10K–P), implying loss or degradation of these proteins during extraction from confluent cultures, low abundance levels resulting in a failure of LC-MS to identify and quantify them or too stringent pre-defined peptide/protein identification criteria. As observed with F-actin cytoskeletal filament staining, GDNF treatment was associated with more continuous intercellular contracts and few intercellular gaps at the human BNB *in vitro*, as previously published.<sup>19</sup>

## Discussion

Using well-established assays of endothelial barrier function, this study demonstrates the role of intracellular MAPK signaling in GDNF-mediated

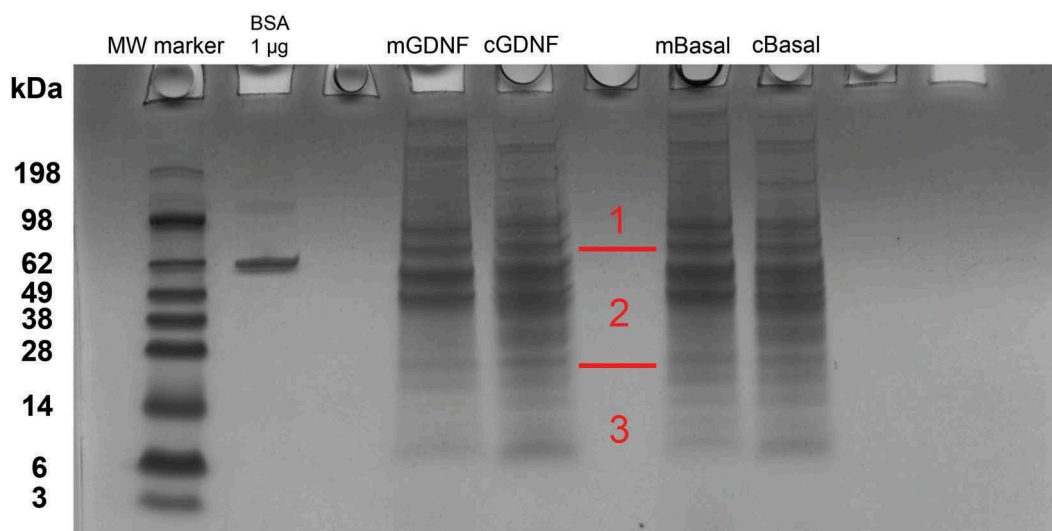


**Figure 9.** GDNF-treated and untreated pHEndEC cytosolic and membrane protein expression following serum withdrawal. A digital photograph of the Colloidal Coomassie-stained 10% Bis-Tris gel following SDS-PAGE of pHEndEC cytosolic and membrane protein extracts shows the three sections of the gel cut from top to bottom prior to trypsin digestion (indicated in red), with subsequent LC-MS, protein identification and quantification, as described in the Materials and Methods section. MW = molecular weight; BSA = bovine serum albumin; mGDNF = membrane protein extract, GDNF-treated; cGDNF = cytosolic protein extract, GDNF-treated; mBasal = membrane protein extract, basal conditions; cBasal = cytosolic protein extract, basal conditions.

**Table 1.** Comparative quantitative proteomics of selected junctional complex-associated proteins. Proteomic quantification of selected proteins based on normalized average total ion current of cytosolic and membrane protein fractions of confluent pHEndECs 48 hours following serum withdrawal without (basal) and with GDNF treatment shows a total increase in CTNNA1 expression associated with a reduction in cytosolic expression and increase in membrane expression mediated by GDNF. There is a diffuse increase in TLN1 cytosolic and membrane expression following GDNF treatment compared to basal conditions. Total ZYX expression was reduced following GDNF treatment associated with reduction in membrane expression with minimal change in cytosolic expression compared to basal conditions. Protein extracts from 2 independent experiments were combined, quantified in triplicate and averaged using the Scaffold software as described in the Materials and Methods section.

Protein	Basal cytosolic	GDNF cytosolic	Fold Change	Basal membrane	GDNF membrane	Fold Change	Basal Total	GDNF Total	Fold change
CTNNA1	50798	39195	0.77	116810	145520	1.25	167608	184715	1.10
TLN1	86205	96750	1.12	119360	146880	1.23	205565	243630	1.18
ZYX	278630	269960	0.97	391860	233520	0.60	670490	503480	0.75

enhancement of human BNB function following serum withdrawal *in vitro*, and also confirms that GDNF signals through RET-tyrosine kinase during this process. The unique cytoskeletal and intercellular junctional complex molecular transcript changes associated with this biological effect was determined using commercially available, validated quantitative PCR arrays, emphasizing the importance of cytoskeletal remodeling, formation of continuous intercellular contracts and the repertoire of transcripts that are involved in forming human BNB adherens and tight junctions *in vitro*, without making assumptions about which components should be studied based on presumed biological function or the most

appropriate internal reference or housekeeping genes for comparative analyses. Similarly, quantitative proteomic analyses of cytosolic and membrane fractions allows identification, relative enumeration and compartmentalization of proteins implicated in forming the restrictive human BNB *in vitro* under the influence of exogenous GDNF in a more comprehensive way.

We demonstrated using quantitative proteomics that certain GDNF-induced cytoskeletal or junctional complex transcripts were not translated to protein (e.g. CTNNA2) *in vitro*, and that specific proteins may be diffusely upregulated (e.g. TLN1) or undergo relative translocation from the cytosol to intercellular membranes (e.g. CTNNA1)



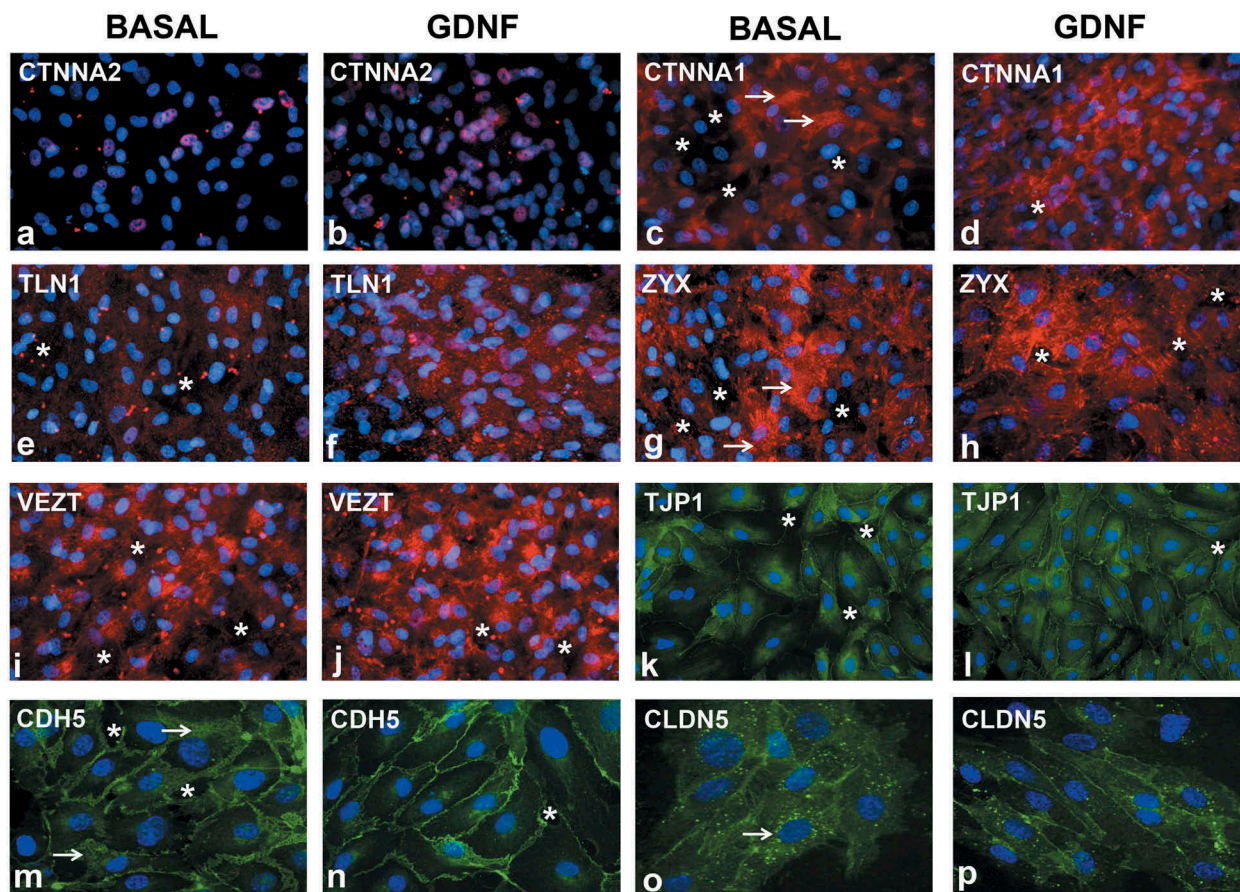


**Figure 10.** Effect of GDNF on selected human BNB junctional complex proteins following serum withdrawal. Representative digital indirect fluorescent immunocytochemistry photomicrographs of visually confluent pHEndECs *in vitro* 48 hours after serum withdrawal shows restricted nuclear CTNNA2 expression in GDNF-untreated (basal, A) and treated cultures (B) with foci of intense cytoplasmic CTNNA1 expression in basal (white arrows, C) compared to more diffuse increased cytoplasmic CTNNA1 expression following GDNF (D). Diffuse punctate cytoplasmic TLN1 expression seen under basal conditions (E) contrasts with more intense diffuse staining seen following GDNF treatment (F). Foci of intense ZYX expression associated with intercellular cytoplasmic projections is seen under basal conditions (white arrows, G) compared to less intense and uniformly more diffuse expression following GDNF treatment (H). Contrary to the PCR array data, there is reduced focal perinuclear and cytosolic VEZT expression under basal conditions (I) compared to GDNF-treated cells (J). Less organized intercellular junctions expressing TJP1 are seen under basal conditions (K) compared to GDNF treatment (L). Similarly, less organized intercellular junctions with broader CDH5 membrane expression is seen under basal conditions (white arrows, M) compared to GDNF-treated pHEndECs (N). CLDN5 intercellular junctional expression is less organized and associated with more intense punctate perinuclear cytoplasmic staining under basal conditions (white arrow, O) compared to expression on more continuous and organized intercellular junctions with GDNF treatment (P). Intercellular gaps (white asterisk), which are more prevalent under basal conditions compared to GDNF-treated pHEndECs, are shown. Positive protein expression = red in A-J and green in K-P, with nuclei depicted in blue. Initial magnification 400X for all photomicrographs.

associated with restrictive intercellular junctional complex formation at the human BNB *in vitro* compared to basal conditions. However, there are limitations with the current quantitative LC-MS analyses as it failed to identify certain intercellular junction proteins in the membrane or cytosolic extracts that were observed by immunocytochemistry. Further work is needed to optimize the membrane protein extraction protocol to facilitate detection of important junctional complex proteins

(e.g. claudins) that would guide further mechanistic studies of the restrictive human BNB *in vitro*. This study supports prior *in vitro* human BNB observations and demonstrates that restrictive barrier function does not simplistically involve upregulation of specific adherens and tight junction proteins alone, but critically involves early cytoskeletal changes required to provide the scaffolding needed for restrictive intercellular junctional complex formation.<sup>32-36</sup> Due to phenotypic and functional



differences between microvascular endothelial cells from different tissues and species, a comprehensive understanding of the molecular determinants and signaling mechanisms implicated in human BNB function in health and disease is biologically relevant, with translational potential to non-traumatic peripheral neuropathies.

This paper also demonstrates the highest published human BNB TEER *in vitro* (in both the growth and post-serum withdrawal phases) using ECIS, applying knowledge that demonstrated the superiority of using GTA-crosslinked RTC as the matrix scaffold for pHEndEC growth and junctional complex formation over RTC alone.<sup>37</sup> Regulation of endothelial barrier function *in vivo* and *in vitro* is known to be influenced by the extracellular matrix composition.<sup>38-40</sup> The mammalian BNB TEER *in vivo* or *in situ* is unknown; however, it may be of the same order of magnitude as the blood-brain barrier. Co-culture with pericytes and/or astrocytes, contact inhibition of endothelial cell proliferation and removal of mitogens from culture media after confluence, as well as the incorporation of shear stress along the longitudinal axis of confluent monolayers typically support formation of tighter intercellular junctions.<sup>41-47</sup> This study did not culture pHEndECs with pericytes or Schwann cells, the glial cell type found in peripheral nerves, apply shear stress to confluent pHEndECs or measure solute permeability under flow conditions. Unlike astrocytes with cerebral microvessels, Schwann cells are not in direct contact with human endoneurial microvessels *in vivo*.<sup>4,5</sup> Specific adaptations are likely needed, guided by *in vivo* and *in situ* observations, to develop a more physiological human BNB model for *in vitro* manipulation with higher translational potential or biological relevance, as observed with a flow-dependent leukocyte-BNB model designed to study peripheral neuroinflammation.<sup>48,49</sup>

Endothelial cells are serum-dependent for attachment, and serum withdrawal is associated with diffuse reduction in continuous intercellular membrane contacts in sub-confluent proliferating cells.<sup>46</sup> However, serum withdrawal is also a well-established technique to suppress growth, induce contact-inhibition and promote intercellular junction formation by confluent epithelial and

endothelial cells *in vitro*.<sup>50-52</sup> The effect of GDNF, RET-tyrosine kinase and MAPK signaling in maintaining a high TEER following serum withdrawal was confirmed at the human BNB *in vitro*. Schwann cells are the primary source of GDNF in peripheral nerves *in vivo*.<sup>12,53,54</sup> The current study suggests that purinergic receptor P2RX6 may be involved in the human BNB endothelial cell response to serum withdrawal due to its high transcript expression levels under basal conditions without exogenous GDNF. This hypothesis is supported by a recent publication that demonstrated activation of Schwann cell P2 type purinergic receptors following sciatic nerve injury that resulted in induced GDNF transcription in adult male Sprague-Dawley rats.<sup>54</sup>

There is evidence supporting the notion that GDNF is a general paracrine regulator of mammalian endothelial tight junctions in restrictive blood-tissue barriers based on work with porcine brain capillary and human brain microvascular cells (blood-brain barrier),<sup>20,23</sup> rat retinal microvascular endothelial cells (inner blood-retinal barrier)<sup>22</sup> and rat testicular microvessels (blood-testis barrier).<sup>24</sup> These specialized endothelial cells express GDNF receptor, GFR $\alpha$ 1 on their cell membranes *in vitro* or *in situ*. There is also evidence that GDNF (secreted by enteric glial cells) regulates the intestinal epithelial barrier *in vitro* and *in vivo*, with a potential role in barrier maturation (via p38 MAPK pathway), wound healing (via cyclic AMP/protein kinase A pathway) and in the pathogenesis of inflammatory bowel disease.<sup>25-28</sup>

GDNF (maximal at 1 ng/mL) demonstrated a minor heparin-dependent increase in pHEndEC proliferation and angiogenesis relative to normal serum-containing basal medium without added growth factors, with no significant effect on sterile micropipette-induced wound healing *in vitro* (which involved an initial phase of endothelial cell migration followed by proliferation that was primarily mediated by vascular endothelial growth factor [VEGF]<sub>A165</sub>).<sup>18</sup> Our study does not support GDNF-mediated pHEndEC proliferation following serum withdrawal based on continuous capacitance measurements as the reason for more restrictive barrier characteristics. Our data imply that GDNF could function as an essential regulator of restrictive barrier formation in peripheral nerve

endoneurium following endothelial cell proliferation and angiogenesis. It is therefore plausible that Schwann cells could directly regulate tight junction formation in endoneurial microvessels during peripheral nerve development and possibly following injury via GDNF secretion. In support of this, we have observed an important role for GDNF in rapidly restoring BNB impermeability to a large macromolecule following non-dissecting sciatic nerve crush injury using a murine conditional GDNF knockout model, independent of CDH5 and CLDN5 expression by indirect fluorescent immunohistochemistry.<sup>55</sup>

Recent published work on the normal adult human BNB transcriptome (deduced by detecting conserved transcripts by both pHEndECs *in vitro* and laser capture microdissected endoneurial microvessels from peripheral nerve biopsies *in situ* by RNA-sequencing) demonstrated a comprehensive repertoire of cytoskeletal and junctional complex transcripts and their associated biological networks. That publication ascertained the expression of at least 133 known intercellular junctional complex transcripts, including 22 tight junction or junction-associated molecules, 45 adherens junction or junction associated molecules, and 52 cell junction-associated or adaptor molecules by the human BNB. Networks/subnetworks associated with intercellular adherens and tight junctions and their organization demonstrated p-values between  $1.9 \times 10^{-63}$  and  $6.7 \times 10^{-4}$ , implying that these are highly significant for human BNB biological function in normal adults.<sup>7</sup>

The human BNB transcriptome, coupled with *in situ* protein expression by endoneurial microvessels in human peripheral nerves, also provides an essential framework for biologically relevant studies to directly verify mechanisms of intercellular junctional complex formation in health and disease using *in vitro* and *in vivo* models. Restoration of the endoneurial microenvironment may be a necessary prerequisite for efficient and efficacious axonal regeneration in peripheral neuropathies, so strategies to locally administer GDNF or increase endogenous GDNF expression by Schwann cells could translate into targeted molecular therapies for these group of disorders (as GDNF also supports peripheral nerve axonal

regeneration), recognizing that a narrow therapeutic window and off-target effects may exist for mitogen-based biologic therapies.<sup>56-58</sup>

In conclusion, we confirm a role for exogenous GDNF in enhancing restrictive human BNB biophysical properties *in vitro* via RET-tyrosine kinase-MAPK signaling, associated with changes in specific cytoskeletal-adaptor-junctional complex transcripts by quantitative real-time PCR and quantitative proteomics, and propose that Schwann cells may facilitate this process *in vivo* during development and following diffuse endoneurial microvessel injury associated with traumatic or toxic peripheral neuropathies. Direct enhancement of intracellular MAPK signaling for therapeutic purposes may prove difficult due to the ubiquitous use of this pathway in multiple cellular processes, including cell survival. Identifying and studying specific proteins such as TLN1 and CTNNA1, and the signaling pathways downstream of MAPK signaling associated with transcription control of essential cytoskeletal and junctional complex genes, mechanisms of cytoskeletal remodeling and protein translocation from the cytosol to intercellular membranes, regulation of cell polarity and intercellular junction complex formation may provide targets for future therapeutic modulation to restore physiological BNB function in adult human peripheral nerves in different disease states.

## Materials and methods

### Phase contrast microscopy and immunocytochemistry

pHEndECs were used throughout this study. Detailed protocols on their isolation, purification, culture and characterization have been published.<sup>59</sup> Cryopreserved pHEndECs were expanded and seeded at 200,000 cells per well in 6-well CellBIND® tissue culture plates (Corning, catalog # 3335) coated with glutaraldehyde (GTA)-crosslinked Type I rat tail collagen (RTC) (Corning catalog # 354236) followed by RTC gel coating. Serum withdrawal (with or without 1 ng/mL GDNF in RPMI-1640 + 1% BSA) was performed 5 days after culturing to confluence with regular growth medium (RPMI-1640, 10%

NuSerum, 10% fetal bovine serum, 1% vitamin solution, 1% non-essential amino acid solution, 1% sodium pyruvate, 1% penicillin-streptomycin, 2 mM L-glutamine, 10 mM HEPES buffer, and enriched with 50  $\mu\text{g}/\text{mL}$  endothelial cell growth supplement, 1 ng/mL human recombinant basic fibroblast growth factor and 10 U/mL heparin, from the same vendors), as previously published.<sup>19,59</sup> Serum withdrawal was performed for 48 hours by carefully aspirating growth medium ~120 hours after initial pHEndEC plating and replacing with serum-deficient RPMI-1640 + 1% bovine serum albumin (BSA), with and without human recombinant GDNF (PeproTech catalog #450–10), as previously published.<sup>19</sup> Phase contrast digital photomicrographs were taken using a Zeiss Axiocam MRc 5 digital camera mounted on a Zeiss Axiovert 40 inverted microscope to observe morphological changes prior to and associated with serum withdrawal with and without exogenous GDNF.

Rhodamine-phalloidin immunocytochemistry to detect F-actin cytoskeletal filaments was performed according to the manufacturer's protocol, as previously published.<sup>19</sup> Briefly, pHEndECs were seeded at 30,000 cells/cm<sup>2</sup> and cultured to confluence on GTA-crosslinked RTC-coated borosilicate glass coverslips placed in 24-well Corning costar tissue culture plates for 5 days. Serum withdrawal was performed as described above. Cells were fixed in 4% paraformaldehyde (PFA) in 1X PBS, permeabilized with 0.1% Triton-X-100 in 1X PBS at  $-20^{\circ}\text{C}$ , blocked with 1% BSA in 1X PBS, incubated with 1:40 stock of rhodamine-phalloidin (Invitrogen, catalog #R415) diluted in blocking medium and treated with 0.45  $\mu\text{M}$  DAPI to detect nuclei. All washes were performed with 1X PBS. Air-dried coverslips were mounted in Vectashield and visualized using a Zeiss Axioskop epifluorescent microscope equipped with an Axiocam MRc 5 digital camera. Images were initially processed using the Zeiss Axiovision software program.

Junctional complex-associated protein pHEndEC immunocytochemistry was performed to determine expression and changes in protein distribution associated with GDNF treatment following serum withdrawal, modifying a previously published protocol.<sup>19</sup> As described above, pHEndECs were cultured to confluence and

underwent serum withdrawal on GTA-crosslinked RTC-coated borosilicate glass coverslips placed in 24-well Corning costar tissue culture plates. Medium were aspirated from the 24-well plates and washed with Dulbecco's PBS (D-PBS: 0.1 g  $\text{MgCl}_2 \cdot 6\text{H}_2\text{O}$  + 0.132 g  $\text{CaCl}_2 \cdot 2\text{H}_2\text{O}$  in 1000 mL 1X PBS). Cells were fixed with 4% PFA in 1X PBS for 10 minutes, washed with D-PBS and permeabilized with freshly made methanol/acetone 1:1 v/v (for  $\alpha$ 2-catenin [CTNNA2], talin-1 [TLN1], zyxin [ZYG1], vezatin [VEZT], cadherin-5 [CDH5] and claudin-5 [CLDN5]) or 0.1% Triton-X-100 (for zona occludens-1 [TJP1] and  $\alpha$ 1-catenin [CTNNA1]) for 3--5 minutes at  $-20^{\circ}\text{C}$ .

After washing with D-PBS and air drying for 5 minutes at room temperature, cells were blocked with 2% normal goat serum (NGS) in 1X PBS for 30 minutes followed by incubation with the following primary antibodies in 2% NGS in 1X PBS for 60 minutes at room temperature in the dark: Rabbit anti-human CTNNA2 IgG (1:50 dilution; ThermoFisher Scientific catalog # MA514963), rabbit anti-human TLN1 IgG (1  $\mu\text{g}/\text{mL}$ ; Abcam catalog #71333), rabbit anti-human ZYG1 IgG (133  $\mu\text{g}/\text{mL}$ ; ThermoFisher Scientific catalog # PA1-25162), rabbit anti-human VEZT IgG (4  $\mu\text{g}/\text{mL}$ ; ThermoFisher Scientific catalog # PA5-52115), mouse anti-human CDH5 IgG1 (4  $\mu\text{g}/\text{mL}$ ; Santa Cruz Biotechnology catalog # sc-9989), mouse anti-human CLDN5 IgG1 (10  $\mu\text{g}/\text{mL}$ ; ThermoFisher Scientific catalog # 35-2500), rabbit anti-human TJP1 IgG (5  $\mu\text{g}/\text{mL}$ ; ThermoFisher Scientific catalog # 61-7300), and mouse anti-human CTNNA1 IgG1 (2  $\mu\text{g}/\text{mL}$ ; ThermoFisher Scientific catalog # 13-9700).

Following washes with 2% NGS in 1X PBS, cells were appropriately incubated with the following secondary antibodies in 2% NGS in 1X PBS for 60 minutes at room temperature in the dark: Goat anti-rabbit IgG (H + L) Alexa Fluor 594 (4  $\mu\text{g}/\text{mL}$ ; ThermoFisher Scientific catalog # A11037), goat anti-mouse IgG (H + L) Alexa Fluor 594 (4  $\mu\text{g}/\text{mL}$ ; ThermoFisher Scientific catalog # A11005), goat anti-rabbit IgG (H + L)-FITC (2  $\mu\text{g}/\text{mL}$ ; SouthernBiotech catalog #4050-02) or goat anti-mouse IgG (H + L)-FITC (2  $\mu\text{g}/\text{mL}$ ; SouthernBiotech catalog #1031-02). Following washes with 2% NGS in 1XPBS, cells were treated

with 0.45  $\mu\text{M}$  DAPI to detect nuclei, washed with D-PBS and mounted on a glass microscope slide with Vectashield. pHEndECs were visualized using a Zeiss Axioskop epifluorescent microscope equipped with an Axiocam MRc 5 digital camera and initially processed using the Zeiss Axiovision software program or a Nikon Eclipse Ci-S Upright epifluorescent microscope with a D5-Qi2 camera and initially processed Nikon NIS-Elements AR software program. Photomicrographs were merged using Adobe Photoshop as needed and mounted into a single figure using Microsoft PowerPoint prior to final image generation with Adobe Photoshop.

### **Human in vitro BNB proteomics**

Total cellular cytoplasmic proteins were extracted from pHEndEC cultures initially grown to confluence in 6-well rat tail collagen-coated Corning CellBIND<sup>®</sup> tissue culture plates, followed by treatment with serum-deficient basal medium containing human recombinant GDNF for 48 hours, to discover possible downstream intracellular signaling pathways. Extraction was performed by gentle scraping in cold lysis buffer (10 mM potassium chloride+ 10 mM HEPES+ 0.1 mM ethylene diamine tetraacetic acid+ 0.1 mM ethylene glycol tetraacetic acid+ 1 mM dithiothreitol+ 0.5 mM phenylmethanesulfonyl fluoride+ 0.05% tergitol<sup>®</sup> nonyl phenoxy polyethoxyethanol-40 in deionized distilled water) containing protease inhibitor cocktail (1:300 dilution; Sigma-Aldrich catalog # P8340) on ice, followed by brief sonication and centrifugation at 18,000 g for 20 min at 4°C, as previously published.<sup>19,60</sup> Protein extracts were quantified using the Bradford Coomassie assay and stored at  $-80^{\circ}\text{C}$ .

200  $\mu\text{L}$  of the pHEndEC cytoplasmic protein extract sample was concentrated down to  $\sim 40$   $\mu\text{L}$  in 50 mM ammonium bicarbonate, and separated by sodium dodecyl sulfate-polyacrylamide gel electrophoresis (SDS-PAGE) using a 10% Bis-Tris gel in duplicate (20  $\mu\text{L}$ , or 12.6  $\mu\text{g}$  per lane), with a lane containing 100 ng BSA (as an internal assay control) and an independent lane containing molecular weight markers also included on the gel. The gel was stained overnight with Colloidal Coomassie. Both lanes were cut into 6 pieces from the top to bottom, and each

piece/fraction was digested separately with trypsin overnight. The digests from both pHEndEC protein extract lanes were combined prior to LC-MS analysis by the University of Alabama Comprehensive Cancer Center Mass Spectrometry/Proteomics Shared Facility, using an established protocol.<sup>61</sup>

The XCalibur RAW files collected in profile mode were centroided and converted to MzXML using ReADW v. 3.5.1. The .mgf files were created using MzXML2Search for all scans with a precursor mass between 300 Da and 1200 Da. The data were searched using SEQUEST version 27, revision 12 set for maximum missed cleavages of five, trypsin digestion, variable modification +57 on C (carbamidomethyl) and +16 on M (oxidation) and fixed modification +1000002 on X. For the fragment-ion mass tolerance, 0.00 Da was used. Searches were performed with the mjdb\_human2-201304 database (29,243 entries). The resulting list of the generated peptide IDs was filtered using Scaffold version 4.4.1 (Proteome software, Portland, OR), using an experiment-wide grouping with binary peptide-protein weight strategy. The filter cut-off values were set with peptide count ( $>2$  AA's), peptide probability set to 80% C.I.,  $\geq 2$  peptides/protein, and protein probabilities set to  $> 99\%$  C.I., with a final peptide false detection rate (FDR) of  $< 2.1\%$  and protein FDR of 0.0%. Protein annotation was performed using Gene Ontology (<http://www.genontology.org/>).

In another series of experiments, pHEndEC cultures were grown to confluence in four 75  $\text{cm}^2$  GTA-crossedlinked rat tail collagen-coated Corning CellBIND<sup>®</sup> tissue culture flasks, followed by treatment with serum-deficient basal medium with or without human recombinant GDNF for 48 hours (two flasks each) as described previously. The aim was to comprehensively identify membrane and cytosolic proteins associated with cytoskeletal remodeling and junctional complex formation and determine relative changes induced by GDNF. Membrane and cytosolic proteins from each flask (with  $\sim 3\text{--}4 \times 10^6$  cells) were extracted using the Mem-PER<sup>TM</sup> membrane protein extraction kit (Thermo Scientific catalog #89842), according to the manufacturer's protocol for adherent mammalian cells. Membrane and cytosolic fractions from the basal and GDNF-



treated confluent pHEndEC cultures (2 each) were pooled, quantified using the Bradford Coomassie assay and stored at  $-80^{\circ}\text{C}$ .

200  $\mu\text{L}$  of the membrane samples and 1 mL of the cytosolic samples were concentrated down using 3k MWCO filter columns into PBS. The concentrated samples were quantified using Bradford Coomassie assay. 8  $\mu\text{g}$  per sample (maximum loading amount for the least concentrated sample) were separated by SDS-PAGE using a 10% Bis-Tris gel, with a lane containing 1  $\mu\text{g}$  BSA (internal assay control) and an independent lane containing molecular weight markers also included on the gel. The gel was stained overnight with Colloidal Coomassie. Each sample lane was digested in 3 fractions with trypsin overnight. LC-MS analysis was performed to identify and quantify proteins in each sample by the normalized average total ion current method using Scaffold version 4.8.7 (Proteome software, Portland, OR).

The data were searched using SEQUEST version 27, revision 12 set for maximum missed cleavages of five, trypsin digestion, variable modification + 57 on C (carbamidomethyl) and + 16 on M (oxidation) and fixed modification + 1000002 on X. For the fragment-ion mass tolerance, 0.00 Da was used. Searches were performed with the *mjdb\_human2-20150516* database (24,325 entries). The resulting list of the generated peptide IDs was filtered using Scaffold version 4.8.7, using an experiment-wide grouping with binary peptide-protein weight strategy. The filter cut-off values were set with peptide count ( $> 2$  AA's), peptide probability set to 80% C.I.,  $\geq 2$  peptides/protein, and protein probabilities set to  $> 99\%$  C.I., with a final peptide false detection rate (FDR) of  $< 2.1\%$  and protein FDR of 0.0%. Protein annotation was performed on FASTA-formatted files using UniRef/NREF (UniProt: <https://www.uniprot.org/>). Identified proteins were quantified using Scaffold software. Normalized average total ion current sums the intensity of all the peaks contained in the MS/MS spectrum of an identified protein, with the area under the peak being directly proportional to the height of the peak. Quantitative data were obtained in triplicate and averaged for each identified protein. Selected junctional complex associated proteins were selected for initial comparative analyses between confluent

GDNF-treated and basal pHEndECs following serum withdrawal for 48 hours.

### **Electric cell-substrate impedance sensing measurement of transendothelial electrical resistance**

ECIS Cultureware™ disposable electrode arrays consisting of 8-well cell culture plates (growth surface area  $0.8\text{ cm}^2$ ) with gold electrodes (8W10E+, Applied Biophysics) were treated with 200  $\mu\text{L}$  of 10 mM cysteine in ddH<sub>2</sub>O. The arrays were coated with a 1:1 mix of 0.2% GTA in 1X PBS and 50  $\mu\text{g}/\text{mL}$  Type I RTC (Corning catalog # 354236) in 0.02 N acetic acid for 1 hour at room temperature, washed twice with 1X PBS and treated with 2% glycine for 5 minutes to neutralize residual GTA and then washed again. The arrays were subsequently RTC gel-coated in ammonia vapor as previously described.<sup>19,37,59</sup> Recently expanded cryopreserved pHEndECs were plated at 30,000 cells in each coated 8W10E+array well and allowed to grow to confluence at  $37^{\circ}\text{C}$  in a specialized humidified incubator containing 95% air/5% CO<sub>2</sub> for 5 days in regular growth medium, with medium changed every 2–3 days, as previously published.<sup>18,19,37,59,62</sup>

Impedance, TEER and capacitance were continuously measured in each independent well at 4000 Hz at 30-second intervals using a 16-electrode array station attached to an ECIS Z $\theta$  system with its specialized data acquisition and analysis software (Applied Biophysics) throughout the duration of the assay. ECIS generates complex impedance spectroscopy data by employing a constant alternating current over adherent cells grown over specialized electrodes, and impedance (and as consequence, electrical resistance in Ohms [ $\Omega$ ]) is automatically calculated in each well using by the software program from changes in voltage between these electrodes for the entire cell layer.<sup>29</sup> 4000 Hz was chosen to determine both junctional (paracellular) and transcellular electrical resistance. This is a more relevant physiological TEER measure comparable to the *in vivo* situation than junctional resistance alone. Stabilized baseline well resistance prior to initial pHEndEC plating in each well was subtracted from measured resistances after seeding by the software program to ascertain

BNB TEER. Pauses and verification of proper electrode contact were performed with medium changes only. Serum withdrawal was performed for 48 hours by carefully aspirating growth medium ~ 120 hours after initial pHEndEC plating and replacing with serum-deficient RPMI-1640 + 1% bovine serum albumin (BSA), as previously published.<sup>19</sup>

Confluent pHEndECs were left untreated (basal condition) or treated with 1 ng/mL human recombinant GDNF (PeproTech catalog #450–10) with or without specific cell permeable inhibitors against RET-tyrosine kinase (SPP86 [1-Isopropyl-3-(phenylethynyl)-1H-pyrazolo[3,4-d]pyrimidin-4-amine], Sigma Aldrich catalog # SML1435, 1  $\mu$ M), MEK1 (PD98059, 2 $\beta$ -Amino-3 $\beta$ -methoxyflavone, EMD Millipore Calbiochem catalog # 513000, 5  $\mu$ M) and ERK 1/2 (FR180204, 5-(2-Phenyl-pyrazolo[1,5-a]pyridin-3-yl)-1H-pyrazolo[3,4-c]pyridazin-3-ylamine, EMD Millipore Calbiochem catalog # 328007, 1  $\mu$ M) in triplicate, guided by previously published protocols.<sup>19,21</sup> Adding these inhibitors to cultured confluent pHEndECs without growth medium or added mitogens induces cell death within 6–24 hours.

TEER just prior to serum withdrawal in each well (A), TEER 48 hours after serum withdrawal in each well (B) and the maximum GDNF-mediated TEER achieved during serum withdrawal (C) were extracted from the data files for each experiment and used to calculate TEER increase (D) in  $\Omega$  and % maximal TEER (i.e. persistence, E) at 48 hours following serum withdrawal as follows:

$$D = B - A$$

$$E = [(B - A)/(C - A)] \times 100\%$$

Three independent experiments, performed in triplicate (total of 9 wells per experimental condition), were analyzed to determine the role of MAPK signaling in GDNF-mediated BNB TEER change.

### Solute permeability assessments

6.5 mm diameter polyester membrane Transwell® inserts with 3.0  $\mu$ m pore size (Corning, catalog #

3472) placed in 24-well tissue culture plates were coated with GTA-crosslinked RTC followed by RTC gel coating, as previously described. pHEndECs were seeded and serum withdrawal performed 5 days after culture in regular growth medium. The permeability of confluent, optimally cultured pHEndEC layers to sodium fluorescein (Na-FITC, molecular weight 376 Da) and fluoresceinated high molecular weight (70 kDa) dextran (dextran-70-FITC) were independently determined across each transwell inserts 48 hours later, using previously published methods.<sup>19,37,59</sup> Briefly, 100  $\mu$ L of a 1 mg/mL solution of either Na-FITC or dextran-70-FITC in 1X PBS (warmed to 37°C) was added into each transwell insert placed in a 24-well tissue culture plate containing 600  $\mu$ L of basal medium at 37°C for 15 minutes in a humidified incubator containing 95% air/5% CO<sub>2</sub>. The concentration of Na-FITC or FITC-dextran-70 kDa in the receiving well was determined fluorometrically against a standard curve of known concentrations using a Synergy 2 Multi-Mode microplate Reader (BioTeK, North Carolina, USA). The permeability coefficient is directly proportional to the ratio of solute that permeates the transwell membrane to the input, expressed as a percentage of the input.<sup>59</sup>

Transwell inserts and wells were left untreated or treated with 1 ng/mL GDNF with or without the previously described specific inhibitors against RET-tyrosine kinase (1–10  $\mu$ M), MEK1 (5–100  $\mu$ M) and ERK 1/2 (10–250  $\mu$ M) in triplicate at the time of serum withdrawal to establish the most effective inhibitory concentration in these assays. Data were normalized as percentages relative to basal permeability following serum withdrawal without added GDNF to facilitate comparisons between different experiments, as previously published.<sup>19</sup> A total of 5 independent experiments (with 15 transwell inserts per experimental condition) were analyzed for each solute studied.

### Human adherens junction and tight junction quantitative real-time PCR arrays

pHEndECs were seeded at 200,000 cells per well in 6-well CellBIND® tissue culture plates (Corning, catalog # 3335) coated with GTA-crosslinked

RTC followed by RTC gel coating. Serum withdrawal (with or without 1 ng/mL GDNF in RPMI-1640 + 1% BSA) was performed 5 days after culturing to confluence with regular growth medium as previously described. 48 hours after serum withdrawal, pHEndEC total RNA was extracted from each well using TRIzol® reagent according to the manufacturer's instructions.<sup>19,37,59</sup> Total RNA was quantified using a NANODrop 2000C spectrophotometer (Thermo Fisher Scientific). 400 ng of total RNA were used for reverse transcription of each sample using a complimentary DNA (cDNA) conversion kit. cDNA was used in combination with RT<sup>2</sup> SYBR® Green qPCR Mastermix (Qiagen catalog # 330529) for quantitative real-time PCR performed to ascertain the transcript changes associated with the GDNF-mediated modulation of human BNB biophysical properties following serum withdrawal *in vitro*.

10 µL of the experimental PCR cocktail was added to each well of the Human Adherens Junction (QIAGEN, catalog # PAHS-146ZA) and Human Tight Junction (QIAGEN, catalog # PAHS-143ZA) RT<sup>2</sup> Profiler PCR Arrays in duplicate. Real-time PCR was performed using a Roche LightCycler 480 (384-well block) with SYBR green detection (QIAGEN) according to the manufacturer's instructions. The following thermal profile was applied: Denature: 1 cycle at 95°C for 10 minutes. Amplification cycle: 45 cycles at 95°C for 15 seconds followed by 60°C for 1 minute. A melting curve analysis was performed to verify PCR specificity: 95°C for 1 minute, 65°C for 2 minutes (optics off) and 65°C to 95°C at 2°C/min afterwards. Quantitative PCR data were obtained using Roche LightCycler 480 software and analyzed by QIAGEN's PCR Array Data Analysis Web Portal.

$C_T$  values were exported to a Microsoft Office Excel file to create a table of  $C_T$  values for each transcript per experiment, differentiating between basal and GDNF-treated conditions. Tables from two independent experiments performed in duplicate were then uploaded to the data analysis web portal at <http://www.qiagen.com/geneglobe>. Data quality control was performed based on PCR array reproducibility, reverse transcription efficiency and genomic DNA contamination.  $C_T$  values were normalized based on an automatic selection of an optimal set of internal control/

housekeeping/normalization reference genes for the analysis from the available housekeeping gene panel incorporated in each PCR Array. The data analysis web portal calculated fold change/regulation using the  $\Delta\Delta C_T$  method, in which  $\Delta C_T$  was calculated between gene of interest and an average of reference genes, followed by  $\Delta\Delta C_T$  calculations ( $\Delta C_T$  (GDNF) –  $\Delta C_T$  (basal)). Fold Change was then calculated using the  $2^{(-\Delta\Delta C_T)}$  formula, with a fold regulation cut-off of  $\pm 2$  and  $p < 0.05$  used to determine biologically significant transcript changes that occur at the human BNB as a consequence of exogenous GDNF treatment following serum withdrawal *in vitro* relative to basal conditions.

### Statistical analyses

Statistical analyses were performed and graphs were generated using Prism software (GraphPad Software, Inc.; La Jolla, CA). Unless otherwise stated, all data are expressed as mean  $\pm$  standard error of mean (SEM). Significance was determined using the paired or unpaired Welch's t-test, as data sets were determined to be parametric based on tests of skewness and kurtosis, with  $p < 0.05$  indicative of statistical significance.

### Acknowledgments

This work was supported by the National Institutes of Health (NIH) [grant number R01 NS075212]. The content is solely the responsibility of the authors and does not necessarily represent the official views of the NIH. The funding sources had no involvement in the conduct of the research, manuscript preparation, data collection/analyses or decision to submit this work for publication.

### Funding

This work was supported by the National Institute of Neurological Disorders and Stroke [R01 NS075212].

### Potential conflicts of interest

E.E.U. has a non-exclusive commercial license managed by Baylor Licensing Group (Baylor College of Medicine, Houston, TX) to market an SV40 large T-antigen immortalized human endoneurial endothelial cell line (not used in this study) and has received royalties from Springer Science +

Business Media for an edited book on laboratory protocols that describes a flow-dependent *in vitro* BNB assay (not used in this study) that utilizes the primary human endoneurial endothelial cells. C.D. has nothing to disclose.

## References

- Greathouse KM, Palladino SP, Dong C, Helton ES, Ubogu EE. Modeling leukocyte trafficking at the human blood-nerve barrier in vitro and in vivo geared towards targeted molecular therapies for peripheral neuroinflammation. *J Neuroinflammation*. 2016;13:3. doi:10.1186/s12974-015-0469-3.
- Olsson Y. Microenvironment of the peripheral nervous system under normal and pathological conditions. *Crit Rev Neurobiol*. 1990;5:265–311.
- Mizisin AP, Weerasuriya A. Homeostatic regulation of the endoneurial microenvironment during development, aging and in response to trauma, disease and toxic insult. *Acta Neuropathol*. 2011;121:291–312. doi:10.1007/s00401-010-0783-x.
- Reina MA, Lopez A, Villanueva MC, De Andres JA, Maches F. [The blood-nerve barrier in peripheral nerves]. *Rev Esp Anestesiol Reanim*. 2003;50:80–86.
- Reina MA, Lopez A, Villanueva MC, de Andres JA, Leon GI. [Morphology of peripheral nerves, their sheaths, and their vascularization]. *Rev Esp Anestesiol Reanim*. 2000;47:464–475.
- Ubogu EE. The molecular and biophysical characterization of the human blood-nerve barrier: current concepts. *J Vasc Res*. 2013;50:289–303. doi:10.1159/000353293.
- Palladino SP, Helton ES, Jain P, Dong C, Crowley MR, Crossman DK, Ubogu EE. The human blood-nerve barrier transcriptome. *Sci Rep*. 2017;7:17477. doi:10.1038/s41598-017-17475-y.
- Beck KD, Valverde J, Alexi T, Poulsen K, Moffat B, Vandlen RA, Rosenthal A, Hefti F. Mesencephalic dopaminergic neurons protected by GDNF from axotomy-induced degeneration in the adult brain. *Nature*. 1995;373:339–341. doi:10.1038/373339a0.
- Bennett DL, Michael GJ, Ramachandran N, Munson JB, Averill S, Yan Q, McMahon SB, Priestley JV. A distinct subgroup of small DRG cells express GDNF receptor components and GDNF is protective for these neurons after nerve injury. *J Neurosci*. 1998;18:3059–3072.
- Henderson CE, Phillips HS, Pollock RA, Davies AM, Lemeulle C, Armanini M, Simmons L, Moffet B, Vandlen RA, Simpson LC Corrected to Simmons L, et al. GDNF: a potent survival factor for motoneurons present in peripheral nerve and muscle. *Science*. 1994;266:1062–1064.
- Takahashi M. The GDNF/RET signaling pathway and human diseases. *Cytokine Growth Factor Rev*. 2001;12:361–373.
- Trupp M, Ryden M, Jornvall H, Funakoshi H, Timmusk T, Arenas E, Ibanez CF. Peripheral expression and biological activities of GDNF, a new neurotrophic factor for avian and mammalian peripheral neurons. *J Cell Biol*. 1995;130:137–148.
- Airaksinen MS, Saarma M. The GDNF family: signaling, biological functions and therapeutic value. *Nat Rev Neurosci*. 2002;3:383–394. doi:10.1038/nrn812.
- Jing S, Wen D, Yu Y, Holst PL, Luo Y, Fang M, Tamir R, Antonio L, Hu Z, Cupples R, et al. GDNF-induced activation of the ret protein tyrosine kinase is mediated by GDNFR-alpha, a novel receptor for GDNF. *Cell*. 1996;85:1113–1124.
- Ibanez CF. Structure and physiology of the RET receptor tyrosine kinase. *Cold Spring Harb Perspect Biol*. 2013;5. doi:10.1101/cshperspect.a009134.
- Ibanez CF, Andressoo JO. Biology of GDNF and its receptors - Relevance for disorders of the central nervous system. *Neurobiol Dis*. 2017;97:80–89. doi:10.1016/j.nbd.2016.01.021.
- Allen SJ, Watson JJ, Shoemark DK, Barua NU, Patel NK. GDNF, NGF and BDNF as therapeutic options for neurodegeneration. *Pharmacol Ther*. 2013;138:155–175. doi:10.1016/j.pharmthera.2013.01.004.
- Reddy CL, Yosef N, Ubogu EE. VEGF-A165 potently induces human blood-nerve barrier endothelial cell proliferation, angiogenesis, and wound healing in vitro. *Cell Mol Neurobiol*. 2013;33:789–801. doi:10.1007/s10571-013-9946-3.
- Yosef N, Ubogu EE. GDNF restores human blood-nerve barrier function via RET tyrosine kinase-mediated cytoskeletal reorganization. *Microvasc Res*. 2012;83:298–310. doi:10.1016/j.mvr.2012.01.005.
- Shimizu F, Sano Y, Saito K, Abe M-A, Maeda T, Haruki H, Kanda T. Pericyte-derived glial cell line-derived neurotrophic factor increase the expression of claudin-5 in the blood-brain barrier and the blood-nerve barrier. *Neurochem Res*. 2012;37:401–409. doi:10.1007/s11064-011-0626-8.
- Ubogu EE. Translational strategies in peripheral neuroinflammation and neurovascular repair. *Transl Neurosci*. 2012;3:373–383. doi:10.2478/s13380-012-0039-4.
- Igarashi Y, Chiba H, Utsumi H, Miyajima H, Ishizaki T, Gotoh T, Kuwahara K, Tobioka H, Satoh M, Mori M, et al. Expression of receptors for glial cell line-derived neurotrophic factor (GDNF) and neurturin in the inner blood-retinal barrier of rats. *Cell Struct Funct*. 2000;25:237–241.
- Igarashi Y, Utsumi H, Chiba H, Yamada-Sasamori Y, Tobioka H, Kamimura Y, Furuuchi K, Kokai Y, Nakagawa T, Mori M, et al. Glial cell line-derived neurotrophic factor induces barrier function of endothelial cells forming the blood-brain barrier. *Biochem Biophys Res Commun*. 1999;261:108–112. doi:10.1006/bbrc.1999.0992.
- Kamimura Y, Chiba H, Utsumi H, Gotoh T, Tobioka H, Sawada N. Barrier function of microvessels



- and roles of glial cell line-derived neurotrophic factor in the rat testis. *Med Electron Microsc.* 2002;35:139–145. doi:10.1007/s007950200017.
25. Meir M, Flemming S, Burkard N, Bergauer L, Metzger M, Germer C-T, Schlegel N. Glial cell line-derived neurotrophic factor promotes barrier maturation and wound healing in intestinal epithelial cells in vitro. *Am J Physiol Gastrointest Liver Physiol.* 2015;309:G613–24. doi:10.1152/ajpgi.00357.2014.
  26. Brun P, Giron MC, Qesari M, Porzionato A, Caputi V, Zoppellaro C, Banzato S, Grillo AR, Spagnol L, De Caro R, et al. Toll-like receptor 2 regulates intestinal inflammation by controlling integrity of the enteric nervous system. *Gastroenterology.* 2013;145:1323–1333. doi:10.1053/j.gastro.2013.08.047.
  27. Steinkamp M, Geerling I, Seufferlein T, von Boyen G, Egger B, Grossmann J, Ludwig L, Adler G, Reinshagen M. Glial-derived neurotrophic factor regulates apoptosis in colonic epithelial cells. *Gastroenterology.* 2003;124:1748–1757.
  28. Meir M, Flemming S, Burkard N, Wagner J, Germer C-T, Schlegel N. The glial cell-line derived neurotrophic factor: a novel regulator of intestinal barrier function in health and disease. *Am J Physiol Gastrointest Liver Physiol.* 2016;310:G1118–23. doi:10.1152/ajpgi.00125.2016.
  29. Szulcek R, Bogaard HJ, van Nieuw Amerongen GP. Electric cell-substrate impedance sensing for the quantification of endothelial proliferation, barrier function, and motility. *J Vis Exp.* 2014. doi:10.3791/51300.
  30. Glass R, Loesch A, Bodin P, Burnstock G. P2X4 and P2X6 receptors associate with VE-cadherin in human endothelial cells. *Cell Mol Life Sci.* 2002;59:870–881.
  31. Sauteur L, Affolter M, Belting HG. Distinct and redundant functions of Esam and VE-cadherin during vascular morphogenesis. *Development.* 2017;144:1554–1565. doi:10.1242/dev.140038.
  32. Hartsock A, Nelson WJ. Adherens and tight junctions: structure, function and connections to the actin cytoskeleton. *Biochim Biophys Acta.* 2008;1778:660–669. doi:10.1016/j.bbamem.2007.07.012.
  33. Zihni C, Mills C, Matter K, Balda MS. Tight junctions: from simple barriers to multifunctional molecular gates. *Nat Rev Mol Cell Biol.* 2016;17:564–580. doi:10.1038/nrm.2016.80.
  34. Stamatovic SM, Johnson AM, Keep RF, Andjelkovic AV. Junctional proteins of the blood-brain barrier: new insights into function and dysfunction. *Tissue Barriers.* 2016;4:e1154641. doi:10.1080/21688370.2016.1154641.
  35. Cerutti C, Ridley AJ. Endothelial cell-cell adhesion and signaling. *Exp Cell Res.* 2017;358:31–38. doi:10.1016/j.yexcr.2017.06.003.
  36. Sluysmans S, Vasileva E, Spadaro D, Shah J, Rouaud F, Citi S. The role of apical cell-cell junctions and associated cytoskeleton in mechanotransduction. *Biol Cell.* 2017;109:139–161. doi:10.1111/boc.201600075.
  37. Yosef N, Ubogu EE. An immortalized human blood-nerve barrier endothelial cell line for in vitro permeability studies. *Cell Mol Neurobiol.* 2013;33:175–186. doi:10.1007/s10571-012-9882-7.
  38. Liebner S, Czapalla CJ, Wolburg H. Current concepts of blood-brain barrier development. *Int J Dev Biol.* 2011;55:467–476. doi:10.1387/ijdb.103224sl.
  39. Menezes MJ, McClenahan FK, Leiton CV, Aranmolate A, Shan X, Colognato H. The extracellular matrix protein laminin alpha2 regulates the maturation and function of the blood-brain barrier. *J Neurosci.* 2014;34:15260–15280. doi:10.1523/JNEUROSCI.3678-13.2014.
  40. Zobel K, Hansen U, Galla HJ. Blood-brain barrier properties in vitro depend on composition and assembly of endogenous extracellular matrices. *Cell Tissue Res.* 2016;365:233–245. doi:10.1007/s00441-016-2397-7.
  41. Santaguida S, Janigro D, Hossain M, Oby E, Rapp E, Cucullo L. Side by side comparison between dynamic versus static models of blood-brain barrier in vitro: a permeability study. *Brain Res.* 2006;1109:1–13. doi:10.1016/j.brainres.2006.06.027.
  42. Shimizu F, Sano Y, Abe M-A, Maeda T, Ohtsuki S, Terasaki T, Kanda T. Peripheral nerve pericytes modify the blood-nerve barrier function and tight junctional molecules through the secretion of various soluble factors. *J Cell Physiol.* 2011;226:255–266. doi:10.1002/jcp.22337.
  43. Appelt-Menzel A, Cubukova A, Günther K, Edenhofer F, Piontek J, Krause G, Stüber T, Walles H, Neuhaus W, Metzger M. Establishment of a human blood-brain barrier co-culture model mimicking the neurovascular unit using induced pluri- and multipotent stem cells. *Stem Cell Rep.* 2017;8:894–906. doi:10.1016/j.stemcr.2017.02.021.
  44. Wang YI, Abaci HE, Shuler ML. Microfluidic blood-brain barrier model provides in vivo-like barrier properties for drug permeability screening. *Biotechnol Bioeng.* 2017;114:184–194. doi:10.1002/bit.26045.
  45. Dejana E, Orsenigo F, Molendini C, Baluk P, McDonald DM. Organization and signaling of endothelial cell-to-cell junctions in various regions of the blood and lymphatic vascular trees. *Cell Tissue Res.* 2009;335:17–25. doi:10.1007/s00441-008-0694-5.
  46. Norris WD, Steele JG, Johnson G, Underwood PA. Serum enhancement of human endothelial cell attachment to and spreading on collagens I and IV does not require serum fibronectin or vitronectin. *J Cell Sci.* 1990;95(Pt 2):255–262.
  47. Qian T, Maguire SE, Canfield SG, Bao X, Olson WR, Shusta EV, Palecek SP. Directed differentiation of human pluripotent stem cells to blood-brain barrier endothelial cells. *Sci Adv.* 2017;3:e1701679. doi:10.1126/sciadv.1701679.
  48. Dong C, Greathouse KM, Beacham RL, Palladino SP, Helton ES, Ubogu EE. Fibronectin connecting

- segment-1 peptide inhibits pathogenic leukocyte trafficking and inflammatory demyelination in experimental models of chronic inflammatory demyelinating polyradiculoneuropathy. *Exp Neurol.* 2017;292:35–45. doi:10.1016/j.expneurol.2017.02.012.
49. Dong C, Palladino SP, Helton ES, Ubogu EE. The pathogenic relevance of alphaM-integrin in Guillain-Barre syndrome. *Acta Neuropathol.* 2016;132:739–752. doi:10.1007/s00401-016-1599-0.
  50. Schneider C, King RM, Philipson L. Genes specifically expressed at growth arrest of mammalian cells. *Cell.* 1988;54:787–793.
  51. Nelson PJ, Daniel TO. Emerging targets: molecular mechanisms of cell contact-mediated growth control. *Kidney Int.* 2002;61:S99–105. doi:10.1046/j.1523-1755.2002.0610s1099.x.
  52. Nighot PK, Hu CA, Ma TY. Autophagy enhances intestinal epithelial tight junction barrier function by targeting claudin-2 protein degradation. *J Biol Chem.* 2015;290:7234–7246. doi:10.1074/jbc.M114.597492.
  53. Naveilhan P, ElShamy WM, Ernfors P. Differential regulation of mRNAs for GDNF and its receptors Ret and GDNFR alpha after sciatic nerve lesion in the mouse. *Eur J Neurosci.* 1997;9:1450–1460.
  54. Xu P, Rosen KM, Hedstrom K, Rey O, Guha S, Hart C, Corfas G. Nerve injury induces glial cell line-derived neurotrophic factor (GDNF) expression in Schwann cells through purinergic signaling and the PKC-PKD pathway. *Glia.* 2013;61:1029–1040. doi:10.1002/glia.22491.
  55. Dong C, Helton ES, Zhou P, Ouyang X, d'Anglemont de Tassigny X, Pascual A, López-Barneo J, Ubogu EE. Glial-derived neurotrophic factor is essential for blood-nerve barrier functional recovery in an experimental murine model of traumatic peripheral neuropathy. *Tissue Barriers.* 2018;6:1–22. doi:10.1080/21688370.2018.1479570.
  56. Ee X, Yan Y, Hunter DA, Schellhardt L, Sakiyama-Elbert SE, Mackinnon SE, Wood MD. Transgenic SCs expressing GDNF-IRES-DsRed impair nerve regeneration within acellular nerve allografts. *Biotechnol Bioeng.* 2017;114:2121–2130. doi:10.1002/bit.26335.
  57. Wood MD, Gordon T, Kemp SW, Liu EH, Kim H, Shoichet MS, Borschel GH. Functional motor recovery is improved due to local placement of GDNF microspheres after delayed nerve repair. *Biotechnol Bioeng.* 2013;110:1272–1281. doi:10.1002/bit.24800.
  58. Santosa KB, Jesuraj NJ, Viader A, MacEwan M, Newton P, Hunter DA, Mackinnon SE, Johnson PJ. Nerve allografts supplemented with schwann cells overexpressing glial-cell-line-derived neurotrophic factor. *Muscle Nerve.* 2013;47:213–223. doi:10.1002/mus.v47.2.
  59. Yosef N, Xia RH, Ubogu EE. Development and characterization of a novel human in vitro blood-nerve barrier model using primary endoneurial endothelial cells. *J Neuropathol Exp Neurol.* 2010;69:82–97. doi:10.1097/NEN.0b013e3181c84a9a.
  60. Yosef N, Ubogu EE. alpha(M)beta(2)-integrin-intercellular adhesion molecule-1 interactions drive the flow-dependent trafficking of Guillain-Barre syndrome patient derived mononuclear leukocytes at the blood-nerve barrier in vitro. *J Cell Physiol.* 2012;227:3857–3875. doi:10.1002/jcp.24100.
  61. Ma C, Kojima K, Xu N, Mobley J, Zhou L, Yang S-T, Liu XM. Comparative proteomics analysis of high n-butanol producing metabolically engineered *Clostridium tyrobutyricum*. *J Biotechnol.* 2015;193:108–119. doi:10.1016/j.jbiotec.2014.10.036.
  62. Helton ES, Palladino S, Ubogu EE. A novel method for measuring hydraulic conductivity at the human blood-nerve barrier in vitro. *Microvasc Res.* 2017;109:1–6. doi:10.1016/j.mvr.2016.08.005.